IDENTIFICATION OF MATERIAL DAMAGE IN TWO DIMENSIONAL DOMAINS USING SQUID BASED NDE SYSTEM

H.T. BANKS [1] and F. KOJIMA [2]

Abstract

Problems on the identification of two-dimensional spatial domains arising in the detection and characterization of material damage are considered. For electromagnetic nondestructive evaluation systems, observations of the magnetic flux from the front surface are used in a output least-square approach. Parameter estimation techniques based on the method of mappings are discussed and approximation schemes are developed applying a finite-element Galerkin approach. Theoretical convergence results for computational techniques are given and results are applied to numerical experiments to demonstrate the efficacy of the proposed schemes.

1 Introduction

Detection and characterization of small cracks and corrosion embedded in the structures of aircraft are critical issues in the maintenance of aging aircraft. For instance, carbon fiber reinforced plastics (CFRP) have been widely used in the advanced aircraft and, as a result, demand has grown for assessing the structural integrity of structures made from those materials. An important effort on such problems entails quantitative nondestructive evaluation methods in SQUID-based NDE system [1]. It is well known that SQUIDs (superconducting quantum interference devices) have very high sensitivity for magnetic flux measurements. Due to the highly sensitive magnetic flux measurements, inverse analyses on electromagnetic problems are effectively used for detecting and characterizing cracks and delamination. Initial efforts on such inverse problems include nondestructive testing under SQUID measurements using the direct current method [2]. However, the detections of non-through crack and corrosion-like damage by direct current flows are insufficient because of the lack of information for deep-lying effects from vertical component of magnetic flux measurements. Since a skin depth of metal varies according to frequency of flowing current, it is possible to detect the deep-lying flows by controlling the frequency. To this end, SQUID based nondestructive evaluation (NDE) systems using injection current methods have been recently developed [3, 4]. In this paper, we propose a computational method for recovering corrosion-like damage with magnetic flux density data from the SQUID based NDE system with alternating current force. The idea of the method of mapping techniques ([5, 6]) are effectively used in our inversion procedures. Figure 1 illustrates the overall configuration of SQUID based NDE system proposed here. In this

[1]Center for Research in Scientific Computation, North Carolina State University, Raleigh, NC 27695-8205, USA. E-mail: htbanks@unity.ncsu.edu

[2]Graduate School of Science and Technology, Kobe University, 1-1, Rokkodai, Nada-ku, Kobe 657-8501 JAPAN, E-mail: kojima@cs.kobe-u.ac.jp

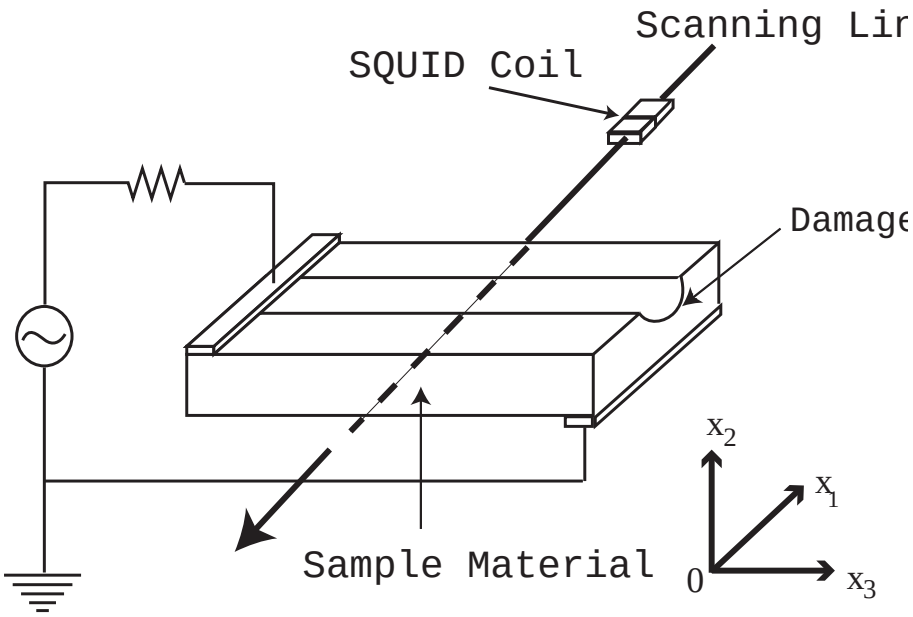

Figure 1: Overall Configuration of SQUID based NDE System

inspection procedure, alternating current forces with multiple angular frequencies are applied to the sample material inspected. A damage corrupts the current flows inside the conductor and we can detect this disturbance from the magnetic flux measurements by the SQUID. The task we consider here is to identify the geometrical shape of the damage from input and output data. Throughout the paper, we assume that the damage is located sufficiently far from both sides of the sample and that the direction of current flow is uniform with respect to the length direction. In Section 2, we consider a two-dimensional mathematical model for inspections based on a SQUID-based NDE system. In Section 3, a direct problem is formulated in variational form in an appropriate Hilbert space. In Section 4, the inverse problem is discussed in the context of a nonlinear output least square problem. The class of admissible parameters are given and the existence of solutions is demonstrated using the idea of the method of mappings. Section 5 is devoted to theoretical convergence for the proposed computational method. Numerical experiments are summarized in Section 6 to demonstrate the efficacy of the proposed method. Related efforts on similar problems are given in [7, 8, 9] where eddy current based techniques are used and the focus is model reduction techniques are opposed to the use of the method of maps employed here.

2 Mathematical Model of Inspection Procedures

Our forward analysis is considered on a cross section of the conducting material sample, i.e.,

$$G_c = \{\ x = (x_1, x_2)\ |\ |x_1| < d_c,\ 0 < x_2 < h_0\ \}$$

as illustrated in Fig. 2. Assuming that the material is of infinite extent in the x_3 direction,

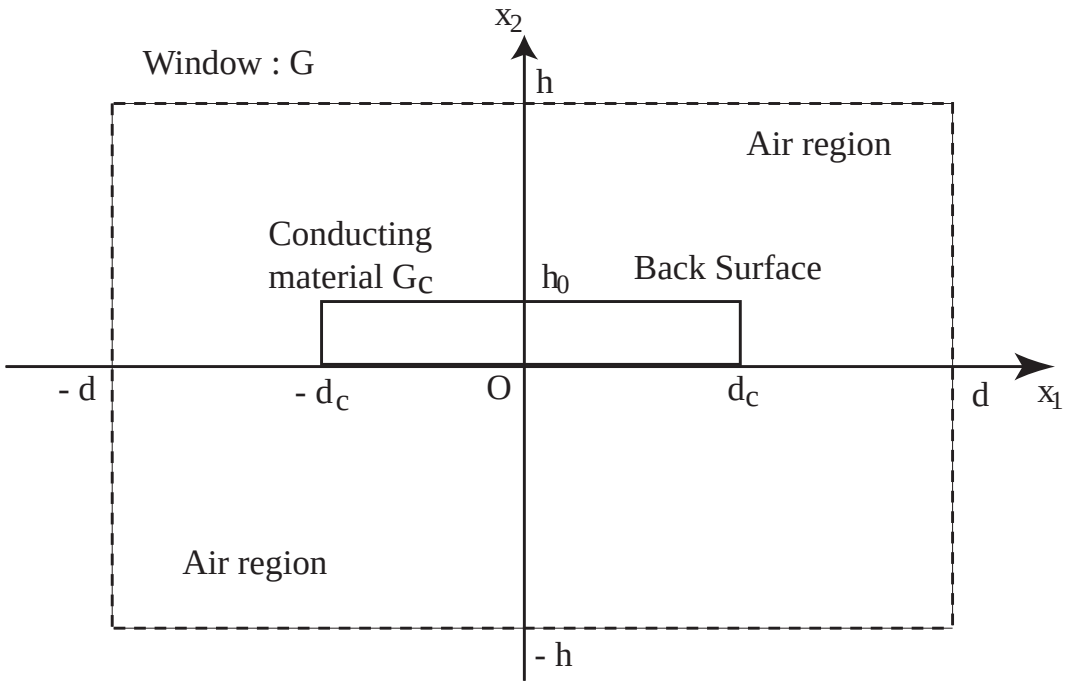

Figure 2: Inspection Area

our problem is defined on an appropriate computational "window" given by

$$G = \{\ x \mid |x_1| < d,\ |x_2| < h\ (h_0 < h < \infty)\ \}\,.$$

A set of alternating current sources $\overline{\mathbf{J}}_i$ with frequencies ω_i is applied to the sample material

$$\overline{\mathbf{J}}_i(t, \mathbf{x}) = (0, 0, J_s(\mathbf{x}))^T \cos(\omega_i t).$$

The set of applied frequencies $\omega = \{\omega_i\}_{i=1}^{M_o}$ can be determined in accordance with the skin depth condition,

$$\delta = \sqrt{\frac{2}{\sigma\mu\omega}} \tag{1}$$

where μ denotes the magnetic permeability and where σ denotes the electrical conductivity of the sample. Given that skin depth of a metal changes according to frequency of flowing current, it is possible to detect a configuration of deep-lying defects by varying the frequency. For the output, measurements can detect the gain margin and phase change of the voltage using a LCZ meter. This means that the SQUID measurements can be represented as

$$\overline{\mathbf{B}}(t, \mathbf{x}) = \mathbf{B}(\mathbf{x}) \cos(\omega t + \theta(\mathbf{x})).$$

Thus it is natural and convenient that the state variables be described by complex phasor representations. The phasor form of Maxwell's equations is given by

$$\nabla \cdot \mathbf{B} \ = \ 0, \tag{2}$$

$$\nabla \cdot \mathbf{E} = 0, \tag{3}$$
$$\nabla \times \mathbf{E} = -j\omega \mathbf{B}, \tag{4}$$
$$\nabla \times \mathbf{H} = \mathbf{J}. \tag{5}$$

Following a standard approach, we introduce the magnetic vector potential $\mathbf{A} = (A_{x_1}, A_{x_2}, A_{x_3})$ defined by $\mathbf{B} = \nabla \times \mathbf{A}$ and the cross product of Eq. (4) can be replaced by representing $\mathbf{E} + j\omega\mathbf{A}$ as the gradient of a scalar electrical potential ϕ, i. e.,

$$\mathbf{E} = -j\omega\mathbf{A} - \nabla\phi.$$

In conjunction with Ohm's law $\mathbf{J} = \sigma\mathbf{E}$ and the constitutive law $\mathbf{B} = \mu\mathbf{H}$, the system state $\mathbf{A}$ is governed by

$$\nabla \times \frac{1}{\mu}\nabla \times \mathbf{A} = -j\omega\sigma\mathbf{A} - \sigma\nabla\phi \tag{6}$$
$$\nabla \cdot (j\omega\mathbf{A} + \nabla\phi) = 0. \tag{7}$$

We assume here that the sample is of nonmagnetic material, so that the magnetic permeability μ is equal to that of air, i.e., $\mu = \mu_0$. In our formulation, the magnetic vector potential becomes $\mathbf{A} = (0, 0, A_3)$. Therefore, the equation for the component of magnetic vector potential $A_3 = A$ is simply rewritten as

$$-\frac{1}{\mu_0}\nabla^2 A + j\chi_c\sigma\omega A = -\chi_c\sigma\frac{\partial\phi}{\partial x_3}$$

where χ_c denotes the characteristic function of the conducting region G_c. Taking into account that the right side of the above equation is composed of the source current density, it follows that

$$J_s = -\sigma\frac{\partial\phi}{\partial x_3} \quad \text{in } G_c.$$

Consequently we can formulate the two dimensional forward problem in terms of the equation:

$$-\frac{1}{\mu_0}\left(\frac{\partial^2 A(x_1, x_2)}{\partial x_1^2} + \frac{\partial^2 A(x_1, x_2)}{\partial x_2^2}\right) + j\chi_c\sigma\omega A(x_1, x_2) = \chi_c J_s(x_1, x_2). \tag{8}$$

Since the boundaries in the x_2 directions are assumed to be sufficiently far from the sample, we assign a Dirichlet boundary condition on this part of the boundary, i. e.,

$$A = 0 \quad \text{on } S_D \tag{9}$$

where

$$S_D = \{\ x \mid |x_1| < d,\ |x_2| = h\ \}.$$

We also consider the boundaries in the x_1 directions to be sufficiently far from the damage so that Neumann boundary conditions in the x_1 direction can be set as:

$$\frac{\partial A}{\partial n} = 0 \quad \text{on } S_N \tag{10}$$

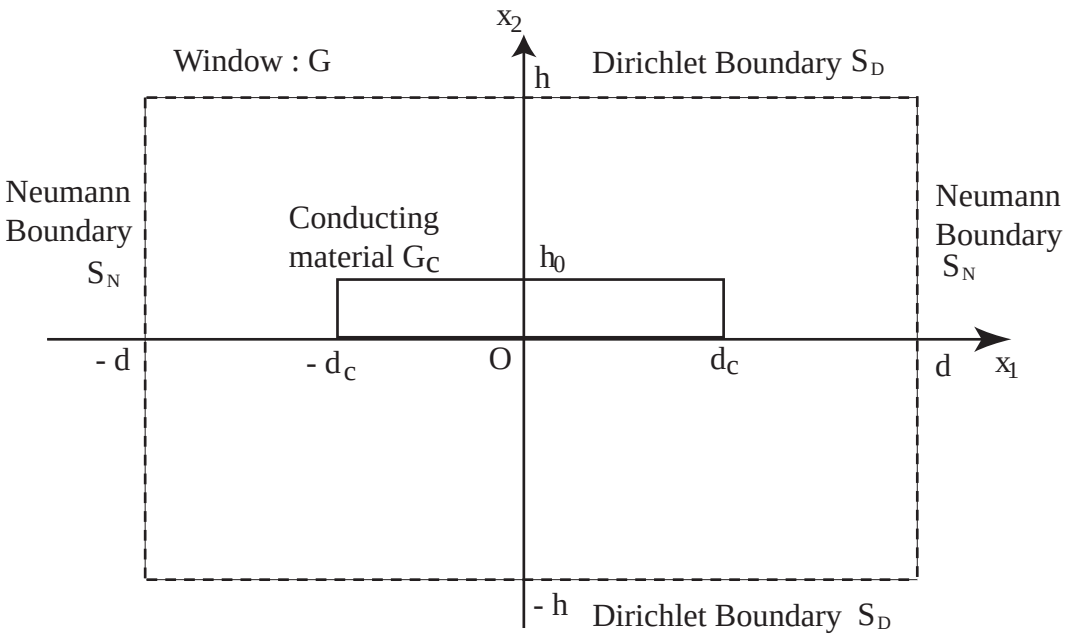

Figure 3: Setting of the boundary condition on the window

where

$$S_N = \{\ x \mid |x_1| = d,\ |x_2| < h\ \}.$$

Figure 3 denotes the boundary conditions on the computational window. In contrast to other magnetic sensors, SQUID measurements can directly detect the magnetic flux densities that are independent of the applied frequencies. Suppose that the scanning strategy is given on the line

$$I = \{\ \mathbf{x} \in G \mid |x_1| \leq r\ (d_c < r),\ x_2 = -h_f\ \},$$

as shown in Fig. 4. Thus the observation mechanism involves data

$$B_2(\mathbf{x}^p) = -\frac{\partial A}{\partial x_1}(\mathbf{x}^p) \quad \text{for } \mathbf{x}^p \in I,\ p = 1, 2, \cdots, m. \tag{11}$$

and the observations are given by

$$z = \mathcal{H}A \quad \in \mathcal{C}^m \tag{12}$$

where $\mathcal{H}$ denotes the bounded operator given by

$$\{\mathcal{H}\}_p = -\frac{1}{|\mathcal{O}^p|}\int_{\mathcal{O}^p} \frac{\partial(\cdot)}{\partial x_1} dx_1 \Big|_{x_2=-h_f} \tag{13}$$

and $\mathcal{O}^p$ denotes the sub-interval of I defined by

$$\mathcal{O}^p \subset \quad (p = 1, 2, \cdots, m). \tag{14}$$

and $|\mathcal{O}^p|$ denotes the length of the sub-interval $\mathcal{O}^p$.

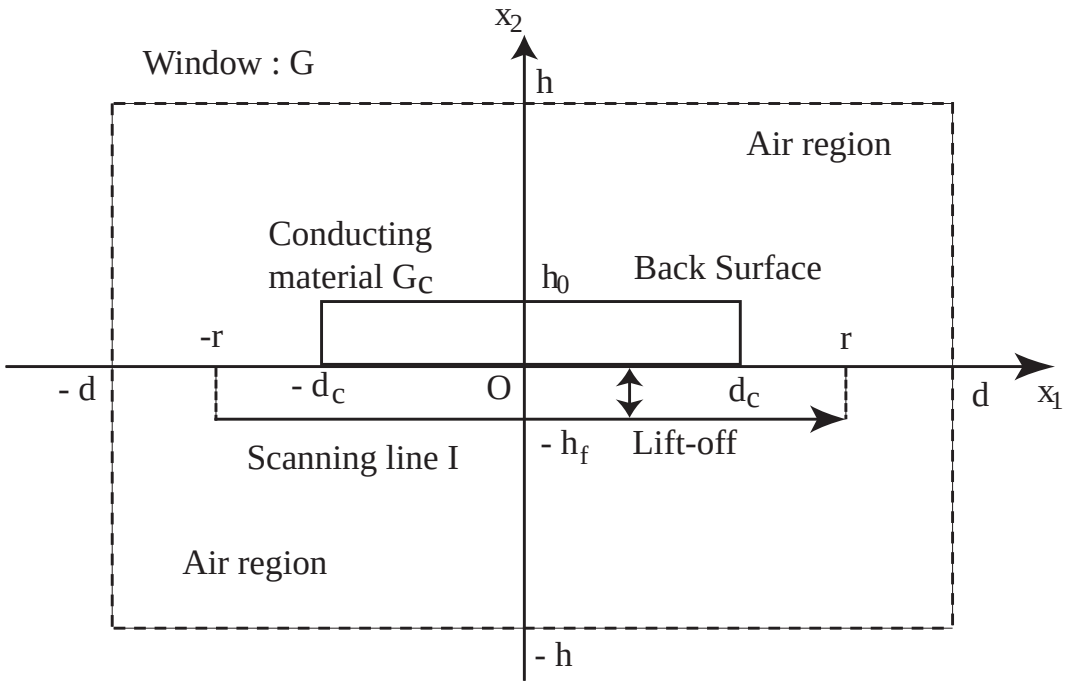

Figure 4: Scanning procedures

3 Weak Formulation

Let $\mathbf{q}$ be a constant vector which characterizes an unknown damage shape where we assume

[**H-0**] The admissible set Q of damage parameters is a compact subset of R^M .

We introduce the "suspect region" $G_s \subset G$ which covers the suspected but unknown damage. More precisely, as depicted in Fig 5, the domain G_s is described by

$$G_s = \{\ x = (x_1, x_2) \mid |x_1| < c, \quad 0 < x_2 < h\ \}.$$

For convenience of discussions, the suspect region G_s is decomposed into two subregions which correspond to the air region G_s^1 and the conducting region G_s^2 and these are parametrized by $\mathbf{q}$. Thus the "window" G is decomposed into three sub-regions G_0, G_s^1 and G_s^2 as follows:

$$G_s = G_s^1(\mathbf{q}) \cup G_s^2(\mathbf{q}), \quad G_0 = G - G_s.$$

We assume the boundary of G is decomposed into

$$\begin{aligned} S_N^0 &= \{\mathbf{x} \mid |x_1| = d,\ |x_2| \le h\ \} \\ S_D^0 &= \{\mathbf{x} \mid c < |x_1| < d,\ x_2 = h\ \} \cup \{\mathbf{x} \mid |x_1| < d,\ x_2 = -h\ \} \\ S_D^1 &= \{\mathbf{x} \mid |x_1| \le c,\ x_2 = h\ \} \end{aligned}$$

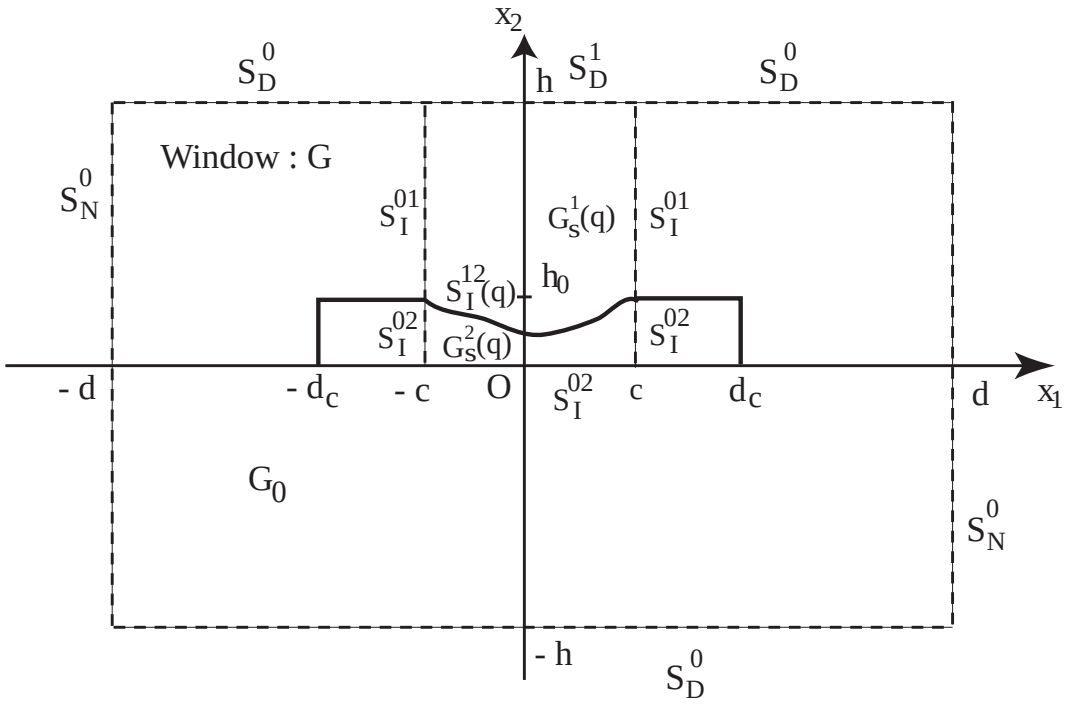

Figure 5: Domain decomposition

and that the interface among sub-regions are defined by

$$\begin{aligned} S_I^{01} &= \{\mathbf{x} \mid |x_1| = c,\ h_0 \le x_2 < h\ \} \\ S_I^{02} &= \{\mathbf{x} \mid |x_1| = c,\ 0 < x_2 < h_0\ \} \cup \{\mathbf{x} \mid |x_1| \le c,\ x_2 = 0\ \} \end{aligned}$$

and S_I^{12} is defined by the interface between $G_s^1(\mathbf{q})$ and $G_s^2(\mathbf{q})$. The form of S_I^{12} will be described in the later discussions. The system state is then denoted by

$$A := A_0 \text{ in } \quad G_0 \quad A := A_i \quad \text{in} \quad G_s^i \quad (i = 1, 2)$$

where

$$A_i := A_i^R + jA_i^I \quad (i = 0, 1, 2).$$

In the sequel, we suppose that the electric conductivity of the conducting material sample has constant value σ_c, i.e.

$$\sigma = \chi_c \sigma_c.$$

Thus the subsystem on G_0 is described by

$$-\frac{1}{\mu_0}\nabla^2 A_0^R - \chi_c\sigma_c\omega A_0^I = \chi_c J_s \tag{15}$$

$$-\frac{1}{\mu_0}\nabla^2 A_0^I + \chi_c\sigma_c\omega A_0^R = 0 \quad \text{in} \quad G_0 \tag{16}$$

with the boundary condition

$$A_0^R = A_0^I = 0 \qquad \text{on} \quad S_D^0 \tag{17}$$

$$\frac{\partial A_0^R}{\partial n} = \frac{\partial A_0^I}{\partial n} = 0 \qquad \text{on} \quad S_N^0. \tag{18}$$

The subsystems defined on $G_s^1(\mathbf{q})$ and $G_s^2(\mathbf{q})$ are described respectively by

$$\nabla^2 A_1^R = 0 \tag{19}$$

$$\nabla^2 A_1^I = 0 \quad \text{in} \quad G_s^1(\mathbf{q}) \tag{20}$$

with the boundary condition

$$A_1^R = A_1^I = 0 \quad \text{on} \quad S_D^1, \tag{21}$$

and

$$-\frac{1}{\mu_0}\nabla^2 A_2^R - \sigma_c \omega A_2^I = J_s \tag{22}$$

$$-\frac{1}{\mu_0}\nabla^2 A_2^I + \sigma_c \omega A_2^R = 0 \quad \text{in} \quad G_s^2(\mathbf{q}). \tag{23}$$

We also need the interface conditions between G_0, $G_s^1(\mathbf{q})$, and $G_s^2(\mathbf{q})$,

$$A_0^R - A_1^R = A_0^I - A_1^I = 0 \tag{24}$$

$$\frac{\partial A_0^R}{\partial n} - \frac{\partial A_1^R}{\partial n} = \frac{\partial A_0^I}{\partial n} - \frac{\partial A_1^I}{\partial n} = 0 \quad \text{on} \quad S_I^{01} \tag{25}$$

$$A_0^R - A_2^R = A_0^I - A_2^I = 0 \tag{26}$$

$$\frac{\partial A_0^R}{\partial n} - \frac{\partial A_2^R}{\partial n} = \frac{\partial A_0^I}{\partial n} - \frac{\partial A_2^I}{\partial n} = 0 \quad \text{on} \quad S_I^{02} \tag{27}$$

$$A_1^R - A_2^R = A_1^I - A_2^I = 0 \tag{28}$$

$$\frac{\partial A_1^R}{\partial n} - \frac{\partial A_2^R}{\partial n} = \frac{\partial A_1^I}{\partial n} - \frac{\partial A_2^I}{\partial n} = 0 \quad \text{on} \quad S_I^{12}(\mathbf{q}). \tag{29}$$

Let φ be in the set

$$V_q = \{\ \varphi \in H^1(G_0 \cup G_s^1(\mathbf{q}) \cup G_s^2(\mathbf{q})) \mid \varphi = 0 \text{ on } S_D^0 \cup S_D^1\ \}$$

endowed with the norm

$$\|\varphi\|^2 := \iint_{G_0 \cup G_s^1(\mathbf{q}) \cup G_s^2(\mathbf{q})} |\nabla \varphi|^2 \, dx_1 dx_2.$$

Let us set

$$\vec{\varphi} := (\varphi^R, \varphi^I) \in V_q \times V_q.$$

Then, for any $\vec{\varphi}, \vec{\psi} \in V_q \times V_q$, we define the bilinear form on $V_q \times V_q$

$$\begin{aligned} a(\mathbf{q})(\vec{\varphi}, \vec{\psi}) \ := \ & \frac{1}{\mu_0} \iint_{G_0 \cup G_s^1(\mathbf{q}) \cup G_s^2(\mathbf{q})} \left(\nabla \varphi^R \cdot \nabla \psi^R + \nabla \varphi^I \cdot \nabla \psi^I \right) dx_1 dx_2 \\ & - \omega \iint_{G_0 \cup G_s^2(\mathbf{q})} \chi_c \sigma_c \varphi^I \psi^R dx_1 dx_2 \\ & + \omega \iint_{G_0 \cup G_s^2(\mathbf{q})} \chi_c \sigma_c \varphi^R \psi^I dx_1 dx_2 \end{aligned} \tag{30}$$

and the linear form on V_q

$$L(\mathbf{q})(\vec{\varphi}) := \iint_{G_0 \cup G_s^2(\mathbf{q})} \chi_c J_s \varphi^R dx_1 dx_2. \tag{31}$$

Lemma 1: Suppose that

[H-1]: The applied angular frequency ω is properly chosen such that

$$\omega \leq \omega_0 < \infty$$

and that

$$\chi_c J_s \in L^2(G).$$

Then, for every $\mathbf{q} \in Q$, there exists a unique solution $\vec{A}(\mathbf{q}) = (A^R, A^I) \in V_q \times V_q$ which is the solution of

$$a(\mathbf{q})(\vec{A}, \vec{\varphi}) = L(\mathbf{q})(\vec{\varphi}) \quad \text{for} \quad \vec{\varphi} \in V_q \times V_q. \tag{32}$$

Moreover, we have

$$\|\vec{A}(\mathbf{q})\|_{V_q \times V_q} \leq K_1 \|\chi_c J_s\|_{L^2(G)} \tag{33}$$

where K_1 is a constant independent of $\mathbf{q}$.

Proof: For arbitrary $\vec{\varphi} \in V_q \times V_q$, $a(\mathbf{q})$ is $V_q \times V_q$-elliptic with constant $\delta = 1/\mu_0$ since

$$a(\mathbf{q})(\vec{\varphi}, \vec{\varphi}) = \frac{1}{\mu_0} \iint_{G_0 \cup G_s^1(\mathbf{q}) \cup G_s^2(\mathbf{q})} \left(\left| \nabla \varphi^R \right|^2 + \left| \nabla \varphi^I \right|^2 \right) dx_1 dx_2 = \delta \|\vec{\varphi}\|^2_{V_q \times V_q} \tag{34}$$

from which follows the coercivity. For the boundedness, it can be easily checked that

$$\left| a(\mathbf{q})(\vec{\varphi}, \vec{\psi}) \right| \leq \gamma \left\| \vec{\varphi} \right\|_{V_q \times V_q} \left\| \vec{\psi} \right\|_{V_q \times V_q}. \tag{35}$$

The linear functional $L(\mathbf{q})$ is bounded on $V_q \times V_q$, i.e.,

$$\begin{aligned}
|L(\mathbf{q})(\vec{\varphi})| &= \left| \iint_{G_0} \chi_c J_s \varphi^R dx_1 dx_2 \right| + \left| \iint_{G_s^2(\mathbf{q})} J_s \varphi^R dx_1 dx_2 \right| \\
&\leq \iint_{G_0} \left| \chi_c J_s \varphi^R \right| dx_1 dx_2 + \iint_{G_s^2(\mathbf{q})} \left| J_s \varphi^R \right| dx_1 dx_2 \\
&\leq \left\{ \left(\iint_{G_0} |\chi_c J_s|^2 \, dx_1 dx_2 \right)^{\frac{1}{2}} + \left(\iint_{G_s^2(\mathbf{q})} |J_s|^2 \, dx_1 dx_2 \right)^{\frac{1}{2}} \right\} \\
&\quad \times \|\vec{\varphi}\|_{L^2(G_0 \cup G_s^1(\mathbf{q}) \cup G_s^2(\mathbf{q}))} \\
&\leq M \left\| \vec{\varphi} \right\|_{V_q \times V_q} \quad \text{for} \quad \vec{\varphi} \in V_q \times V_q.
\end{aligned}$$

Applying the Lax-Milgram lemma, for each $\mathbf{q} \in Q$, we find there exists a unique solution $\vec{A}(\mathbf{q}) \in V_q \times V_q$ satisfying (32). Similarly, we have

$$\delta \|\vec{A}(\mathbf{q})\|^2_{V_q \times V_q} \leq a(\mathbf{q})(\vec{A}, \vec{A}) \leq M \|\vec{A}(\mathbf{q})\|_{V_q \times V_q}$$

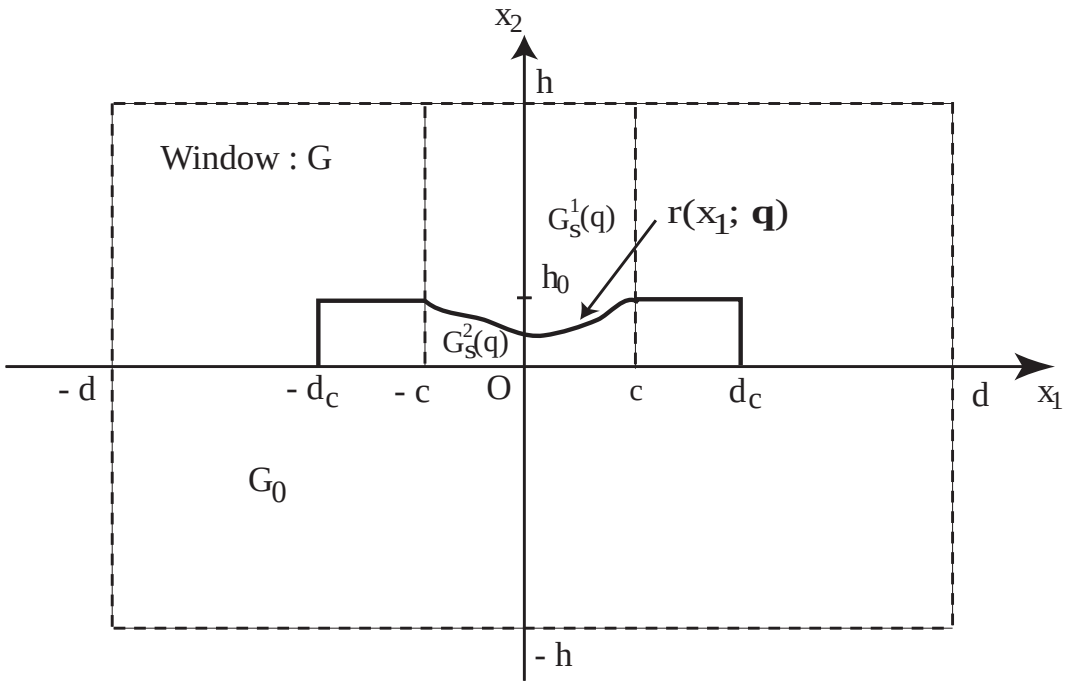

Figure 6: The unknown damage function

from which follows

$$\|\vec{A}(\mathbf{q})\|_{V_q \times V_q} \leq K_1 \quad \text{where} \quad K_1 = \frac{M}{\delta}.$$

This completes the proof.

Remark: In [**H-1**], the upper bound of angular frequency ω_0 can be reasonably set for the inspection. More precisely, the angular frequency ω of the applied current force must be properly chosen by the skin depth condition (1).

4 Admissible Class and Method of Mapping

In this section, we restrict the corrosion-like damage so that it can be represented by a simple parametrized function. The unknown defect shape is characterized by a function

$$x_2 = r(x_1; \mathbf{q}) \quad \text{for} \quad |x_1| \leq c \tag{36}$$

with

$$0 < r(x_1; \mathbf{q}) \leq h_0 \ (< h < \infty) \quad \text{and} \quad r(-c; \mathbf{q}) = r(c; \mathbf{q}) = h_0$$

as depicted in Fig. 6. We describe by $Q \subset R^M$ an admissible set of possible parameter values. The geometrical structure of the damage is restricted by the following hypotheses:

[**H-2**] For each $\mathbf{q} \in Q$, $r(\cdot, \mathbf{q}) \in W_\infty^1(-c, c)$.

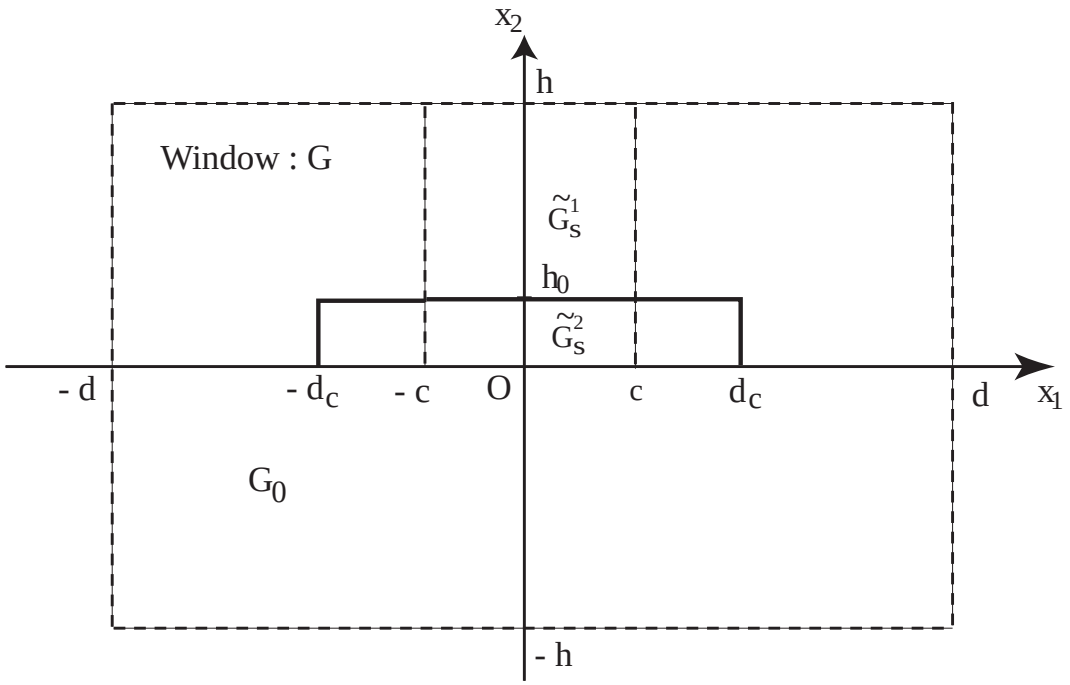

Figure 7: Refence domains

[H-3] There exists a constant β such that, for each $\mathbf{q} \in Q$,

$$0 < \beta \leq r(\cdot, \mathbf{q}).$$

[H-4] There exists a function $dist : Q \times Q \to R^1$ with $dist(\mathbf{q}, \tilde{\mathbf{q}}) \to 0$ as $|\mathbf{q} - \tilde{\mathbf{q}}| \to 0$ such that

$$\|r(\cdot, \mathbf{q}) - r(\cdot, \tilde{\mathbf{q}})\|_{1,\infty} \leq dist(\mathbf{q}, \tilde{\mathbf{q}}) \quad \text{for} \quad \mathbf{q}, \tilde{\mathbf{q}} \in Q.$$

The subregions $G_1(\mathbf{q})$ and $G_2(\mathbf{q})$ given in the previous section can now be explicitly rewritten as

$$G_s^1(\mathbf{q}) = \{ \mathbf{x} \mid |x_1| < c,\ r(x_1, \mathbf{q}) < x_2 < h \}$$

and

$$G_s^2(\mathbf{q}) = \{ \mathbf{x} \mid |x_1| < c,\ 0 < x_2 < r(x_1, \mathbf{q}) \},$$

respectively. Associated with these sub-domains, we define the reference sub-domains as shown in Fig. 7:

$$\tilde{G}_s^1 = \{ \mathbf{x} \mid |x_1| < c,\ h_0 < x_2 < h \}$$
$$\tilde{G}_s^2 = \{ \mathbf{x} \mid |x_1| < c,\ 0 < x_2 < h_0 \}.$$

We introduce the affine mapping:

$$x = T(\mathbf{q})\tilde{x} = \begin{cases} T_1(\mathbf{q})\tilde{x} & \text{for } \tilde{x} \in \tilde{G}_s^1 \\ T_2(\mathbf{q})\tilde{x} & \text{for } \tilde{x} \in \tilde{G}_s^2 \end{cases} \tag{37}$$

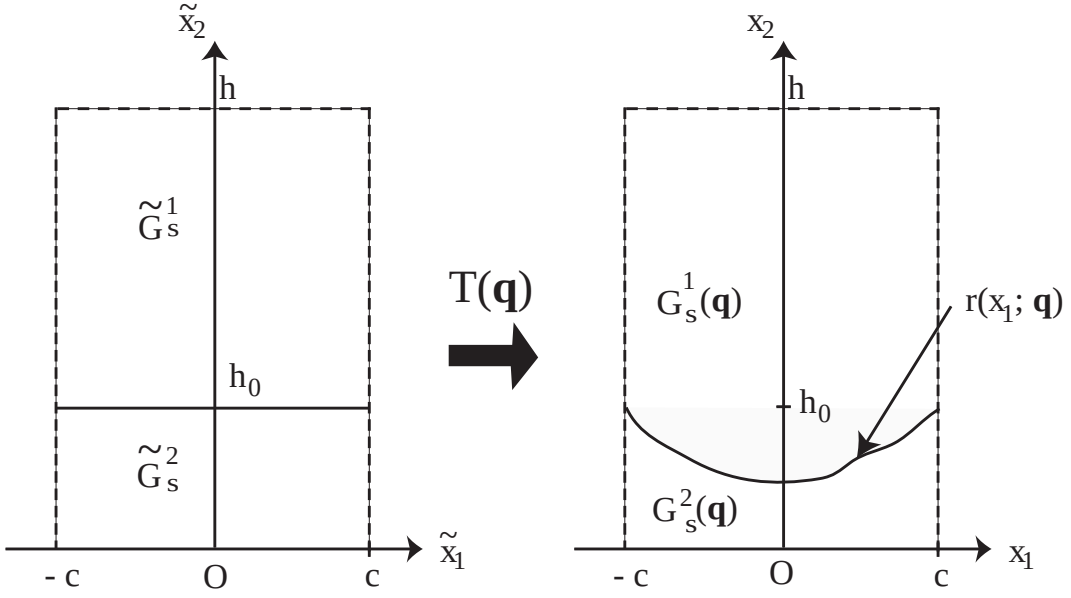

Figure 8: Transformation mapping from the reference domain into the domain with damage

where

$$T_1(\mathbf{q}) = \begin{cases} x_1 = \tilde{x}_1 \\ x_2 = (h - r(\tilde{x}_1;\mathbf{q}))(\tilde{x}_2 - h)/(h - h_0) + h \end{cases}$$

$$T_2(\mathbf{q}) = \begin{cases} x_1 = \tilde{x}_1 \\ x_2 = r(\tilde{x}_1;\mathbf{q})\tilde{x}_2/h_0 \end{cases} .$$

These mappings result in the following identities :

$$G_s^i(\mathbf{q}) = T_i(\mathbf{q}) \circ \tilde{G}_s^i \qquad (i = 1, 2). \tag{38}$$

Figure 8 illustrates the transformation from the reference domain $\tilde{G}_s^1 \cup \tilde{G}_s^2$ into the domain with damage $G_s^1(\mathbf{q}) \cup G_s^2(\mathbf{q})$. Let $\tilde{\varphi}$ be in the set

$$\tilde{V} = \{\ \tilde{\varphi} \in H^1(G_0 \cup \tilde{G}_s^1 \cup \tilde{G}_s^2) \mid \tilde{\varphi} = 0 \text{ on } S_D^0 \cup S_D^1\ \}$$

endowed with the norm

$$\|\tilde{\varphi}\|^2 := \iint_{G_0 \cup \tilde{G}_s^1 \cup \tilde{G}_s^2} |\nabla \tilde{\varphi}|^2 \, d\tilde{x}_1 d\tilde{x}_2.$$

Let us set

$$\vec{\tilde{\varphi}} := (\tilde{\varphi}^R, \tilde{\varphi}^I) \in \tilde{V} \times \tilde{V}.$$

Then, for any $\vec{\tilde{\varphi}}, \vec{\tilde{\psi}} \in \tilde{V} \times \tilde{V}$, the bilinear form $a(\mathbf{q})$ can be represented on $\tilde{V} \times \tilde{V}$ as

$$\tilde{a}(\mathbf{q})(\vec{\tilde{\varphi}}, \vec{\tilde{\psi}}) := \frac{1}{\mu_0} \sum_{i=1}^{2} \iint_{\tilde{G}_s^i} \left\{ \left(\tilde{\nabla}\tilde{\varphi}^R\right) \cdot \left(\tilde{\nabla} T_i(\mathbf{q})\right)^{-t} \left(\tilde{\nabla} T_i(\mathbf{q})\right)^{-1} \left(\tilde{\nabla}\tilde{\psi}^R\right) \right.$$

$$
\begin{aligned}
&+\left(\tilde{\nabla}\tilde{\varphi}^I\right)\cdot\left(\tilde{\nabla}T_i(\mathbf{q})\right)^{-t}\left(\tilde{\nabla}T_i(\mathbf{q})\right)^{-1}\left(\tilde{\nabla}\tilde{\psi}^I\right)\Big\}\det\left|\tilde{\nabla}T_i(\mathbf{q})\right|d\tilde{x}_1d\tilde{x}_2\\
&+\frac{1}{\mu_0}\iint_{G_0}\left\{\left(\tilde{\nabla}\tilde{\varphi}^R\right)\cdot\left(\tilde{\nabla}\tilde{\psi}^R\right)+\left(\tilde{\nabla}\tilde{\varphi}^I\right)\cdot\left(\tilde{\nabla}\tilde{\psi}^I\right)\right\}d\tilde{x}_1d\tilde{x}_2\\
&-\omega\iint_{\tilde{G}_s^2}\sigma_c\tilde{\varphi}^I\tilde{\psi}^R\det\left|\tilde{\nabla}T_2(\mathbf{q})\right|d\tilde{x}_1d\tilde{x}_2\\
&+\omega\iint_{\tilde{G}_s^2}\sigma_c\tilde{\varphi}^R\tilde{\psi}^I\det\left|\tilde{\nabla}T_2(\mathbf{q})\right|d\tilde{x}_1d\tilde{x}_2\\
&-\omega\iint_{G_0}\chi_c\sigma_c\tilde{\varphi}^I\tilde{\psi}^Rd\tilde{x}_1d\tilde{x}_2+\omega\iint_{G_0}\chi_c\sigma_c\tilde{\varphi}^R\tilde{\psi}^Id\tilde{x}_1d\tilde{x}_2. \qquad (39)
\end{aligned}
$$

The linear form on $\tilde{V}$ is also represented by

$$
\tilde{L}(\mathbf{q})(\vec{\tilde{\varphi}}):=\iint_{\tilde{G}_s^2}J_s\tilde{\varphi}^R\det\left|\tilde{\nabla}T_2(\mathbf{q})\right|d\tilde{x}_1d\tilde{x}_2+\iint_{G_0}\chi_cJ_s\tilde{\varphi}^Rd\tilde{x}_1d\tilde{x}_2. \qquad (40)
$$

Noting that

$$
\tilde{\nabla}T_i(\mathbf{q})=\begin{pmatrix}\frac{\partial x_1}{\partial\tilde{x}_1} & \frac{\partial x_1}{\partial\tilde{x}_2}\\ \\ \frac{\partial x_2}{\partial\tilde{x}_1} & \frac{\partial x_2}{\partial\tilde{x}_2}\end{pmatrix},
$$

we obtain

$$
\tilde{\nabla}T_1(\mathbf{q})=\begin{pmatrix}1 & 0\\ \\ -\frac{r'(\tilde{x}_1;\mathbf{q})(\tilde{x}_2-h)}{h-h_0} & \frac{h-r(\tilde{x}_1;\mathbf{q})}{h-h_0}\end{pmatrix}\quad\tilde{\nabla}T_2(\mathbf{q})=\begin{pmatrix}1 & 0\\ \\ -\frac{r'(\tilde{x}_1;\mathbf{q})\tilde{x}_2}{h_0} & \frac{r(\tilde{x}_1;\mathbf{q})}{h_0}\end{pmatrix}.
$$

Similarly, we have

$$
\det\left|\tilde{\nabla}T_1(\mathbf{q})\right|=\frac{h-r(\tilde{x}_1;\mathbf{q})}{h-h_0}\quad\det\left|\tilde{\nabla}T_1(\mathbf{q})\right|=\frac{r(\tilde{x}_1;\mathbf{q})}{h_0}.
$$

Hence the explicit form of Eq. (39) can be represented as

$$
\begin{aligned}
\tilde{a}(\mathbf{q})(\vec{\tilde{\varphi}},\vec{\tilde{\psi}}) \;:=\; &\sum_{i=1}^{2}\iint_{\tilde{G}_s^i}\Bigg\{a_1^i(\mathbf{q})\left(\frac{\partial\tilde{\varphi}^R}{\partial\tilde{x}_1}\frac{\partial\tilde{\psi}^R}{\partial\tilde{x}_1}+\frac{\partial\tilde{\varphi}^I}{\partial\tilde{x}_1}\frac{\partial\tilde{\psi}^I}{\partial\tilde{x}_1}\right)\\
&+a_2^i(\mathbf{q})\left(\frac{\partial\tilde{\varphi}^R}{\partial\tilde{x}_1}\frac{\partial\tilde{\psi}^R}{\partial\tilde{x}_2}+\frac{\partial\tilde{\varphi}^R}{\partial\tilde{x}_2}\frac{\partial\tilde{\psi}^R}{\partial\tilde{x}_1}+\frac{\partial\tilde{\varphi}^I}{\partial\tilde{x}_1}\frac{\partial\tilde{\psi}^I}{\partial\tilde{x}_2}+\frac{\partial\tilde{\varphi}^I}{\partial\tilde{x}_2}\frac{\partial\tilde{\psi}^I}{\partial\tilde{x}_1}\right)\\
&+a_3^i(\mathbf{q})\left(\frac{\partial\tilde{\varphi}^R}{\partial\tilde{x}_2}\frac{\partial\tilde{\psi}^R}{\partial\tilde{x}_2}+\frac{\partial\tilde{\varphi}^I}{\partial\tilde{x}_2}\frac{\partial\tilde{\psi}^I}{\partial\tilde{x}_2}\right)\Bigg\}d\tilde{x}_1d\tilde{x}_2\\
&+\frac{1}{\mu_0}\iint_{G_0}\left(\frac{\partial\tilde{\varphi}^R}{\partial\tilde{x}_1}\frac{\partial\tilde{\psi}^R}{\partial\tilde{x}_1}+\frac{\partial\tilde{\varphi}^I}{\partial\tilde{x}_1}\frac{\partial\tilde{\psi}^I}{\partial\tilde{x}_1}+\frac{\partial\tilde{\varphi}^R}{\partial\tilde{x}_2}\frac{\partial\tilde{\psi}^R}{\partial\tilde{x}_2}+\frac{\partial\tilde{\varphi}^I}{\partial\tilde{x}_2}\frac{\partial\tilde{\psi}^I}{\partial\tilde{x}_2}\right)d\tilde{x}_1d\tilde{x}_2\\
&+\iint_{\tilde{G}_s^2}a_0(\mathbf{q})\left(-\tilde{\varphi}^I\tilde{\psi}^R+\tilde{\varphi}^R\tilde{\psi}^I\right)d\tilde{x}_1d\tilde{x}_2\\
&+\omega\iint_{G_0}\chi_c\sigma_c\left(-\tilde{\varphi}^I\tilde{\psi}^R+\tilde{\varphi}^R\tilde{\psi}^I\right)d\tilde{x}_1d\tilde{x}_2 \qquad (41)
\end{aligned}
$$

where

$$\begin{aligned}
a_1^1(\mathbf{q}) &= \frac{r'(\tilde{x}_1;\mathbf{q})^2(\tilde{x}_2-h)^2+(h-r(\tilde{x}_1;\mathbf{q}))^2}{\mu_0(h-h_0)(h-r(\tilde{x}_1;\mathbf{q}))} \\
a_2^1(\mathbf{q}) &= \frac{r'(\tilde{x}_1;\mathbf{q})(\tilde{x}_2-h)}{\mu_0(h-r(\tilde{x}_1;\mathbf{q}))} \\
a_3^1(\mathbf{q}) &= \frac{h-h_0}{\mu_0(h-r(\tilde{x}_1;\mathbf{q}))} \\
a_1^2(\mathbf{q}) &= \frac{r'(\tilde{x}_1;\mathbf{q})^2\tilde{x}_2^2+r(\tilde{x}_1;\mathbf{q})^2}{\mu_0 h_0 r(\tilde{x}_1;\mathbf{q})} \\
a_2^2(\mathbf{q}) &= -\frac{r'(\tilde{x}_1;\mathbf{q})\tilde{x}_2}{\mu_0 r(\tilde{x}_1;\mathbf{q})} \\
a_3^2(\mathbf{q}) &= \frac{h_0}{\mu_0 r(\tilde{x}_1;\mathbf{q})},
\end{aligned}$$

and where

$$a_0(\mathbf{q}) = \frac{\omega\sigma_c r(\tilde{x}_1;\mathbf{q})}{h_0}.$$

From (40), the transformed linear form can be explicitly rewritten by

$$\tilde{L}(\mathbf{q})(\vec{\tilde{\varphi}}) := \iint_{\tilde{G}_s^2} \frac{J_s r(\tilde{x}_1;\mathbf{q})}{h_0}\tilde{\varphi}^R d\tilde{x}_1 d\tilde{x}_2 + \iint_{G_0} \chi_c J_s \tilde{\varphi}^R d\tilde{x}_1 d\tilde{x}_2. \tag{42}$$

Lemma 2: With the hypotheses **[H-0]** to **[H-4]**, there exist positive constants α, λ, K_2 and K_3 such that, for $\mathbf{q}_1, \mathbf{q}_2 \in Q$, the bilinear form $\tilde{a}(\mathbf{q})(\cdot,\cdot)$ satisfies the following inequalities for all $\vec{\tilde{\varphi}}, \vec{\tilde{\psi}} \in \tilde{V}\times\tilde{V}$:

$$\tilde{a}(\mathbf{q})(\vec{\tilde{\varphi}},\vec{\tilde{\varphi}}) \geq \alpha \left\|\vec{\tilde{\varphi}}\right\|^2_{\tilde{V}\times\tilde{V}} \tag{43}$$

$$\left|\tilde{a}(\mathbf{q})(\vec{\tilde{\varphi}},\vec{\tilde{\psi}})\right| \leq K_2 \left\|\vec{\tilde{\varphi}}\right\|_{\tilde{V}\times\tilde{V}} \left\|\vec{\tilde{\psi}}\right\|_{\tilde{V}\times\tilde{V}} \tag{44}$$

$$\left|\tilde{a}(\mathbf{q})(\vec{\tilde{\varphi}},\vec{\tilde{\psi}}) - \tilde{a}(\tilde{\mathbf{q}})(\vec{\tilde{\varphi}},\vec{\tilde{\psi}})\right| \leq K_3 dist(\mathbf{q},\tilde{\mathbf{q}}) \left\|\vec{\tilde{\varphi}}\right\|_{\tilde{V}\times\tilde{V}} \left\|\vec{\tilde{\psi}}\right\|_{\tilde{V}\times\tilde{V}} \tag{45}$$

where

$$dist(\mathbf{q},\tilde{\mathbf{q}}) \to 0 \qquad \text{as} \qquad |\mathbf{q}-\tilde{\mathbf{q}}| \to 0.$$

Moreover, α, K_2, and K_3 can be chosen as constants which are independent of the parameter vector $\mathbf{q}$.

Proof: It can be easily shown that, with $c_1, c_3 > 0$, any quadratic form satisfies

$$c_1(\xi_1)^2 - 2c_2\xi_1\xi_2 + c_3(\xi_2^2) \geq \frac{c_1c_3-(c_2)^2}{2}\min\left\{(c_1)^{-1},(c_3)^{-1}\right\}(|\xi_1|^2+|\xi_2|^2).$$

From (41), the associated quadratic form for each suspect region $G_s^i (i = 1, 2)$ becomes

$$\begin{aligned}
&\left\{a_1^i(\mathbf{q})(\xi_1^R)^2 + 2a_2^i(\mathbf{q})(\xi_1^R\xi_2^R) + a_3^i(\mathbf{q})(\xi_2^R)^2\right\} \\
&+ \quad \left\{a_1^i(\mathbf{q})(\xi_1^I)^2 + 2a_2^i(\mathbf{q})(\xi_1^I\xi_2^I) + a_3^i(\mathbf{q})(\xi_2^I)^2\right\} \\
&\geq \quad \frac{a_1^i(\mathbf{q})a_3^i(\mathbf{q}) - (a_2^i(\mathbf{q}))^2}{2} \min\left\{(a_1^i(\mathbf{q}))^{-1}, (a_3^i(\mathbf{q}))^{-1}\right\} \\
&\quad \times(|\xi_1^R|^2 + |\xi_2^R|^2 + |\xi_1^I|^2 + |\xi_2^I|^2). \qquad (46)
\end{aligned}$$

We easily find that

$$a_1^i(\mathbf{q})a_3^i(\mathbf{q}) - (a_2^i(\mathbf{q}))^2 = 1 \quad \text{for } i = 1, 2.$$

Under the hypotheses **[H-2]** and **[H-3]**, we admit that

$$\begin{aligned}
(a_1^1(\mathbf{q}))^{-1} &= \frac{\mu_0(h - h_0)(h - r(\tilde{x}_1; \mathbf{q}))}{r'(\tilde{x}_1; \mathbf{q})^2(\tilde{x}_2 - h)^2 + (h - r(\tilde{x}_1; \mathbf{q}))^2} \geq \frac{\mu_0}{M_1 + M_2} \\
(a_3^1(\mathbf{q}))^{-1} &= \frac{\mu_0(h - r(\tilde{x}_1; \mathbf{q}))}{h - h_0} \geq \mu_0
\end{aligned}$$

where

$$M_1 = \sup_{\mathbf{q}\in Q} \sup_{x_1\in[-c,c]} |r'(\tilde{x}_1; \mathbf{q})|^2 \quad M_2 = \left(\frac{h - \beta}{h - h_0}\right)^2 \geq 1.$$

This implies that, for G_s^1,

$$\min\left\{(a_1^1(\mathbf{q}))^{-1}, (a_3^1(\mathbf{q}))^{-1}\right\} \geq \frac{\mu_0}{M_1 + M_2}. \qquad (47)$$

Similarly, noting that

$$\begin{aligned}
(a_1^2(\mathbf{q}))^{-1} &= \frac{\mu_0 h_0 r(\tilde{x}_1; \mathbf{q})}{r'(\tilde{x}_1; \mathbf{q})^2\tilde{x}_2^2 + r(\tilde{x}_1; \mathbf{q})^2} \geq \frac{\mu_0\beta}{h_0(M_1 + 1)} \\
(a_3^2(\mathbf{q}))^{-1} &= \frac{\mu_0 r(\tilde{x}_1; \mathbf{q})}{h_0} \geq \frac{\mu_0\beta}{h_0},
\end{aligned}$$

we obtain

$$\min\left\{(a_1^2(\mathbf{q}))^{-1}, (a_3^2(\mathbf{q}))^{-1}\right\} \geq \frac{\mu_0\beta}{h_0(M_1 + 1)} \quad \text{for } G_s^2. \qquad (48)$$

Choosing the constant as

$$\alpha = \min\left\{\frac{\mu_0}{M_1 + M_2}, \frac{\mu_0\beta}{h_0(M_1 + 1)}, \frac{1}{\mu_0}\right\}$$

which is independent of $\mathbf{q}$, we obtain the coercivity (43) of the transformed sesquilinear form. To prove the boundedness, we note that, under the hypotheses **[H-1]** to **[H-4]**, it follows that

$$\begin{aligned}
\left|a_j^i(\mathbf{q})\right| &\leq \left(\sup_{q\in\mathbf{q}} \sup_{\tilde{G}_s^i} \left|a_j^i(\mathbf{q})\right|^2\right)^{\frac{1}{2}} \quad (= M_2) \quad \text{for } i = 1, 2; j = 1, 2 \\
\left|a_3^i(\mathbf{q})\right| &\leq \max\left\{\frac{h - h_0}{\mu_0(h - \beta)}, \frac{h_0}{\mu_0\beta}\right\} \quad (= M_3) \quad \text{for } i = 1, 2 \\
|a_0(\mathbf{q})| &\leq \omega_0\sigma_c \ (= M_4).
\end{aligned}$$

Thus, by setting as

$$K_2 = \max\left(M_2, M_3, M_4, \mu_0^{-1}\right),$$

we obtain the boundedness (44). To establish the continuity property, we note that, for any $\mathbf{q}, \tilde{\mathbf{q}} \in Q$,

$$\begin{aligned}
&\left|\tilde{a}(\mathbf{q})(\vec{\tilde{\varphi}}, \vec{\tilde{\psi}}) - \tilde{a}(\tilde{\mathbf{q}})(\vec{\tilde{\varphi}}, \vec{\tilde{\psi}})\right| \\
&\leq \sum_{i=1}^{2} \left| \iint_{\tilde{G}_s^i} \left[\left\{a_1^i(\mathbf{q}) - a_1^i(\tilde{\mathbf{q}})\right\} \left(\frac{\partial \tilde{\varphi}^R}{\partial \tilde{x}_1} \frac{\partial \tilde{\psi}^R}{\partial \tilde{x}_1} + \frac{\partial \tilde{\varphi}^I}{\partial \tilde{x}_1} \frac{\partial \tilde{\psi}^I}{\partial \tilde{x}_1} \right) \right.\right. \\
&\quad + \left\{a_2^i(\mathbf{q}) - a_2^i(\tilde{\mathbf{q}})\right\} \left(\frac{\partial \tilde{\varphi}^R}{\partial \tilde{x}_1} \frac{\partial \tilde{\psi}^R}{\partial \tilde{x}_2} + \frac{\partial \tilde{\varphi}^R}{\partial \tilde{x}_2} \frac{\partial \tilde{\psi}^R}{\partial \tilde{x}_1} + \frac{\partial \tilde{\varphi}^I}{\partial \tilde{x}_1} \frac{\partial \tilde{\psi}^I}{\partial \tilde{x}_2} + \frac{\partial \tilde{\varphi}^I}{\partial \tilde{x}_2} \frac{\partial \tilde{\psi}^I}{\partial \tilde{x}_1} \right) \\
&\quad \left.\left. + \left\{a_3^i(\mathbf{q}) - a_3^i(\tilde{\mathbf{q}})\right\} \left(\frac{\partial \tilde{\varphi}^R}{\partial \tilde{x}_2} \frac{\partial \tilde{\psi}^R}{\partial \tilde{x}_2} + \frac{\partial \tilde{\varphi}^I}{\partial \tilde{x}_2} \frac{\partial \tilde{\psi}^I}{\partial \tilde{x}_2} \right) \right] d\tilde{x}_1 d\tilde{x}_2 \right| \\
&\quad + \left| \iint_{\tilde{G}_s^2} \left\{a_0(\mathbf{q}) - a_0(\tilde{\mathbf{q}})\right\} \left(-\tilde{\varphi}^I \tilde{\psi}^R + \tilde{\varphi}^R \tilde{\psi}^I \right) d\tilde{x}_1 d\tilde{x}_2 \right|.
\end{aligned}$$

With the hypotheses **[H-1]** to **[H-4]**, it can be argued that $a_j^i(\mathbf{q})(i = 1, 2; j = 1, 2, 3)$ are continuous in $L^\infty(\tilde{G}_s^i)$. We can thus infer the continuity of the bilinear form (41) with respect to $\mathbf{q} \in Q$. The proof has been completed.

Lemma 3: Let

$$\vec{\tilde{A}}(\mathbf{q}) = \vec{A} \circ T(\mathbf{q})$$

be the transformed system state. Then, with the hypotheses **[H-0]** to **[H-4]**, for every $\mathbf{q} \in Q$, there exists a unique solution

$$\vec{\tilde{A}}(\mathbf{q}) \in \tilde{V} \times \tilde{V} \tag{49}$$

in the sense that

$$\tilde{a}(\mathbf{q})(\vec{\tilde{A}}(\mathbf{q}), \vec{\tilde{\varphi}}) = \tilde{L}(\mathbf{q})(\vec{\tilde{\varphi}}) \quad \text{for} \quad \vec{\tilde{\varphi}} \in \tilde{V} \times \tilde{V}. \tag{50}$$

Moreover the solution $\vec{\tilde{A}}(\mathbf{q})$ in the system on $G = G_0 \cup \tilde{G}_s^1 \cup \tilde{G}_s^2$ is bounded in $\tilde{V} \times \tilde{V}$ uniformly in $\mathbf{q} \in Q$.

Proof: From **Lemma-2** and from (30), (31), (41), and (42), we have that, for $\vec{\varphi} \in V_q \times V_q$ and $\vec{\tilde{\varphi}} \in \tilde{V} \times \tilde{V}$,

$$\alpha \left|\vec{\tilde{\varphi}}\right|_{\tilde{V} \times \tilde{V}}^2 \leq |a(\mathbf{q})(\vec{\varphi}, \vec{\varphi})| \leq K_2 \left|\vec{\tilde{\varphi}}\right|_{\tilde{V} \times \tilde{V}}^2$$

and

$$a(\mathbf{q})(\vec{\varphi}, \vec{\varphi}) = \tilde{a}(\mathbf{q})(\vec{\tilde{\varphi}}, \vec{\tilde{\varphi}}).$$

Taking into account that the constants α and K_4 are independent of the unknown parameter $\mathbf{q}$, this implies that the $V_q \times V_q$-norm is equivalent to the norm of $\tilde{V} \times \tilde{V}$ uniformly in $\mathbf{q} \in Q$. Since, under the hypothesis **(H-1)**,

$$\left|\tilde{L}(\mathbf{q})(\vec{\tilde{\varphi}})\right| \leq K_4 \left\|\vec{\tilde{\varphi}}\right\|_{L^2(G) \times L^2(G)},$$

there exists the solution $\vec{\tilde{A}}$ in $\tilde{V} \times \tilde{V}$ in the sense of (50). The proof has been completed.

Lemma 4: With the hypotheses **[H-0]** to **[H-4]**, $\mathbf{q} \rightarrow \vec{\tilde{A}}(\mathbf{q})$ is continuous from Q to $\tilde{V} \times \tilde{V}$.

Proof: Let $\mathbf{q}^k \rightarrow \mathbf{q}$ in Q and let $\vec{\tilde{A}}(\mathbf{q}^k)$, $\vec{\tilde{A}}(\mathbf{q})$ be the corresponding solutions of (50). Then, from (50), we have

$$\tilde{a}(\mathbf{q}^k)(\vec{\tilde{A}}(\mathbf{q}^k), \vec{\varphi}) - \tilde{a}(\mathbf{q})(\vec{\tilde{A}}(\mathbf{q}), \vec{\varphi}) = [\tilde{L}(\mathbf{q}^k) - \tilde{L}(\mathbf{q})](\vec{\varphi}) \quad \text{for } \forall \vec{\varphi} \in \tilde{V} \times \tilde{V}.$$

Then we may rewrite

$$\tilde{a}(\mathbf{q}^k)(\vec{\tilde{A}}(\mathbf{q}^k) - \vec{\tilde{A}}(\mathbf{q}), \vec{\varphi}) + [\tilde{a}(\mathbf{q}^k) - \tilde{a}(\mathbf{q})](\vec{\tilde{A}}(\mathbf{q}), \vec{\varphi}) = [\tilde{L}(\mathbf{q}^k) - \tilde{L}(\mathbf{q})](\vec{\varphi}) \quad \text{for } \forall \vec{\varphi} \in \tilde{V} \times \tilde{V}.$$

Choosing as $\vec{\varphi} = \vec{\tilde{A}}(\mathbf{q}^k) - \vec{\tilde{A}}(\mathbf{q})$ in $\tilde{V} \times \tilde{V}$ and using (43) and (45) in **Lemma-2**, we find that

$$\alpha |\vec{\tilde{A}}(\mathbf{q}^k) - \vec{\tilde{A}}(\mathbf{q})|^2_{\tilde{V} \times \tilde{V}} \leq dist(\mathbf{q}^k, \mathbf{q}) \left\{ |\chi J_s|_{L^2(G)} + |\vec{\tilde{A}}(\mathbf{q})|^2_{\tilde{V} \times \tilde{V}} \right\} |\vec{\tilde{A}}(\mathbf{q}^k) - \vec{\tilde{A}}(\mathbf{q})|_{\tilde{V} \times \tilde{V}}.$$

This yields the desired continuity, that is,

$$\alpha |\vec{\tilde{A}}(\mathbf{q}^k) - \vec{\tilde{A}}(\mathbf{q})|_{\tilde{V} \times \tilde{V}} \leq dist(\mathbf{q}^k, \mathbf{q}) \left\{ |\chi J_s|_{L^2(G)} + |\vec{\tilde{A}}(\mathbf{q})|^2_{\tilde{V} \times \tilde{V}} \right\} \quad \longrightarrow \ 0 \quad \text{as } \mathbf{q}^k \ \rightarrow \mathbf{q}.$$

The proof has been completed.

The observation for the transformed state $\vec{\tilde{A}}$ can be rewritten by

$$\tilde{z}(\mathbf{q}; \omega) = \tilde{\mathcal{H}} \vec{\tilde{A}}(\mathbf{q}; \omega) \tag{51}$$

where $\tilde{\mathcal{H}} : \tilde{V} \times \tilde{V} \rightarrow R^m \times R^m$ is given by

$$\left[\tilde{\mathcal{H}} \vec{\tilde{\varphi}}\right]_i = -\frac{1}{|\mathcal{O}^p|} \int_{\mathcal{O}^p} \left(\frac{\partial \tilde{\varphi}^R}{\partial \tilde{x}_1}, \frac{\partial \tilde{\varphi}^I}{\partial \tilde{x}_1} \right) d\tilde{x}_1 \Big|_{\tilde{x}_2 = -h_f} \qquad (p = 1, 2, \cdots, m).$$

Figure 9 depicts the procedures for gathering the measurement data from SQUIDs.

Lemma 5: With the hypotheses **[H-0]** to **[H-4]**, the mapping $\mathbf{q} \rightarrow \tilde{z}(\mathbf{q})$ is continuous from Q to $R^m \times R^m$.

Proof: Taking into account that the operator $\tilde{\mathcal{H}}$ belongs to $\mathcal{L}(\tilde{V} \times \tilde{V}; R^m \times R^m)$ for each $\mathbf{q} \in Q$, we see that the above statement follows directly from **Lemma-4**.

The parameter estimation problem is formulated as follows:

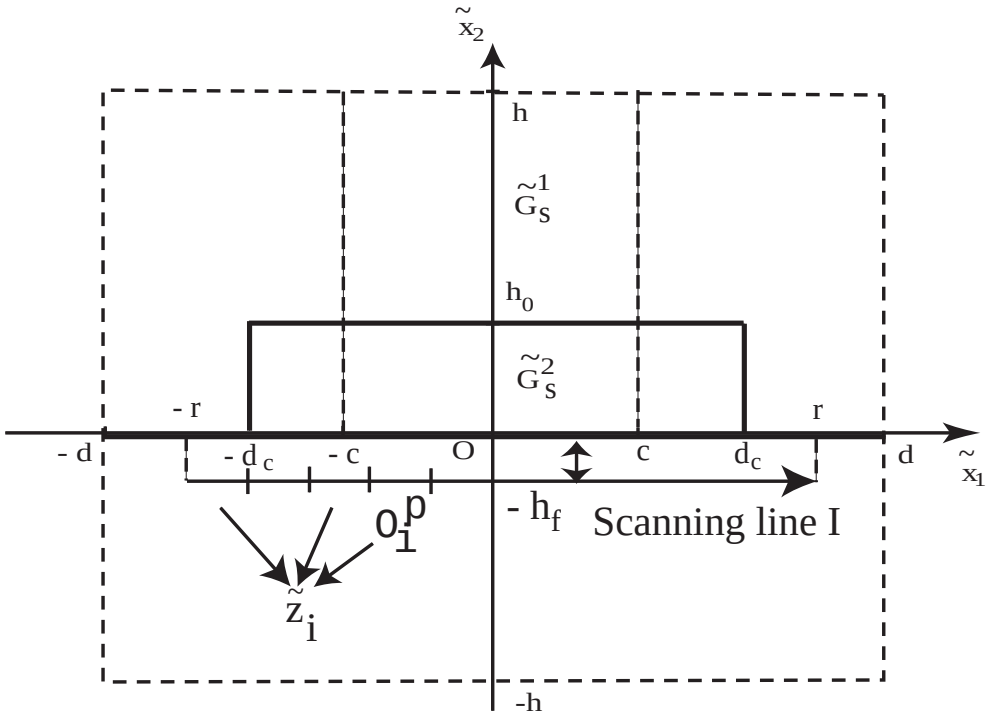

Figure 9: Data acquisition by SQUIDs

Shape Identification Problem **SIDP**:

Given the observed data $\{z_d(\omega_i)\}_{i=1}^{M_o}$ from applying the set of alternating injection currents $\{J_s \cos(\omega_i t)\}_{i=1}^{M_o}$, then find the optimal $\mathbf{q} = \mathbf{q}^*$ which minimizes the fit-to-data functional

$$F(\mathbf{q}) = \frac{1}{2} \sum_{i=1}^{M_o} \left| \tilde{z}(\mathbf{q}; \omega_i) - z_d(\omega_i) \right|^2 \tag{52}$$

with respect to $\mathbf{q} \in Q$ where Q is a compact set of R^M.

Theorem 1: With the hypotheses [**H-0**] - [**H-4**], the problem **SIDP** has at least one solution $\mathbf{q}^* \in Q$.

This follows immediately from the continuity properties given in **Lemma 5** and the compactness of Q.

5 Computational Method and Convergence Analysis

The computational scheme is based on the use of a finite Galerkin approach to construct a sequence of finite dimensional approximating identification problems. To approximate **SIDP**, we choose a sequence of finite dimensional subspace $H^N \times H^N \subset \tilde{V} \times \tilde{V}$ such that

$$\left\| \Pi^N \vec{\varphi} - \vec{\varphi} \right\|_{\tilde{V} \times \tilde{V}} \longrightarrow 0 \quad \text{as} \quad N \to \infty \quad \text{for} \quad \vec{\varphi} \in \tilde{V} \times \tilde{V} \tag{53}$$

where Π^N is the orthogonal projection of

$$\tilde{L}^2(G_0 \cup \tilde{G}_s^1 \cup \tilde{G}_s^2) \times \tilde{L}^2(G_0 \cup \tilde{G}_s^1 \cup \tilde{G}_s^2) \quad \text{onto} \quad H^N \times H^N \tag{54}$$

The approximating system is defined for $\vec{\tilde{A}}^N \in H^N \times H^N$ by

$$\tilde{a}(\mathbf{q})(\vec{\tilde{A}}^N, \vec{\tilde{\varphi}}^N) = \tilde{L}(\mathbf{q})(\vec{\tilde{\varphi}}^N) \quad \text{for} \quad \vec{\tilde{\varphi}}^N \in H^N \times H^N. \tag{55}$$

The observation output for the approximating system can be represented as

$$\tilde{z}^N(\mathbf{q};\omega) = \tilde{\mathcal{H}}\vec{\tilde{A}}^N(\mathbf{q};\omega). \tag{56}$$

Thus the computational method is formulated as follows:

Approximate Shape Identification Problem $(\mathbf{ASIDP})^N$:

Find $\hat{\mathbf{q}}^N \in Q$ which minimizes

$$F^N(\mathbf{q}) = \frac{1}{2}\sum_{i=1}^{M_o} \left|\tilde{z}^N(\mathbf{q};\omega_i) - z_d(\omega_i)\right|^2 \tag{57}$$

Lemma 6: Let $\mathbf{q}^N \to \mathbf{q} \in Q$. Then

$$\vec{\tilde{A}}^N(\mathbf{q}^N) \longrightarrow \vec{\tilde{A}}(\mathbf{q}) \in \tilde{V} \times \tilde{V}. \tag{58}$$

Proof: We have

$$\left\|\vec{\tilde{A}}^N(\mathbf{q}^N) - \vec{\tilde{A}}(\mathbf{q})\right\|_{\tilde{V}\times\tilde{V}} \le \left\|\vec{\tilde{A}}^N(\mathbf{q}^N) - \Pi^N\vec{\tilde{A}}(\mathbf{q})\right\|_{\tilde{V}\times\tilde{V}} + \left\|\Pi^N\vec{\tilde{A}}(\mathbf{q}) - \vec{\tilde{A}}(\mathbf{q})\right\|_{\tilde{V}\times\tilde{V}}.$$

From (53), it suffices to prove

$$\left\|\vec{\tilde{A}}^N(\mathbf{q}^N) - \Pi^N\vec{\tilde{A}}(\mathbf{q})\right\|_{\tilde{V}\times\tilde{V}} \to 0 \quad \text{for} \quad \mathbf{q}^N \to \mathbf{q} \in Q \quad \text{as} \quad N \to \infty.$$

We obtain

$$\tilde{a}(\mathbf{q}^N)(\vec{\tilde{A}}^N(\mathbf{q}^N), \vec{\psi}^N) - \tilde{a}(\mathbf{q})(\vec{\tilde{A}}(\mathbf{q}), \vec{\psi}^N) = [\tilde{L}(\mathbf{q}^N) - \tilde{L}(\mathbf{q})](\vec{\psi}^N) \quad \text{for } \vec{\psi}^N \in H^N \times H^N.$$

Furthermore we have

$$\tilde{a}(\mathbf{q}^N)(\vec{\tilde{A}}^N(\mathbf{q}^N) - \Pi^N\vec{\tilde{A}}(\mathbf{q}), \vec{\psi}^N) + \tilde{a}(\mathbf{q}^N)(\Pi^N\vec{\tilde{A}}(\mathbf{q}) - \vec{\tilde{A}}(\mathbf{q}), \vec{\psi}^N)$$

$$+[\tilde{a}(\mathbf{q}^N) - \tilde{a}(\mathbf{q})](\vec{\tilde{A}}(\mathbf{q}), \vec{\psi}^N) = [\tilde{L}(\mathbf{q}^N) - \tilde{L}(\mathbf{q})](\vec{\psi}^N).$$

Choosing $\vec{\psi}^N = \Delta^N = \vec{\tilde{A}}^N(\mathbf{q}^N) - \Pi^N \vec{\tilde{A}}(\mathbf{q})$, we find that

$$\begin{aligned}\alpha \left\|\Delta^N\right\|^2_{\tilde{V}\times\tilde{V}} &\leq K_2 \left\|\Pi^N \vec{\tilde{A}}(\mathbf{q}) - \vec{\tilde{A}}(\mathbf{q})\right\|_{\tilde{V}\times\tilde{V}} \|\Delta^N\|_{\tilde{V}\times\tilde{V}} \\ &\quad + dist(\mathbf{q}^N, \mathbf{q}) \left\|\vec{\tilde{A}}(\mathbf{q})\right\|_{\tilde{V}\times\tilde{V}} \|\Delta^N\|_{\tilde{V}\times\tilde{V}} + M dist(\mathbf{q}^N, \mathbf{q}) \|\Delta^N\|_{\tilde{V}\times\tilde{V}}.\end{aligned}$$

Consequently, we obtain

$$\alpha \left\|\Delta^N\right\|_{\tilde{V}\times\tilde{V}} \leq K_2 \left\|\Pi^N \vec{\tilde{A}}(\mathbf{q}) - \vec{\tilde{A}}(\mathbf{q})\right\|_{\tilde{V}\times\tilde{V}} + dist(\mathbf{q}^N, \mathbf{q}) \left(\left\|\vec{\tilde{A}}(\mathbf{q})\right\|_{\tilde{V}\times\tilde{V}} + M \right).$$

Thus, given any $\mathbf{q}^N \to \mathbf{q} \in Q$, it follows that $\Delta^N \to 0$ as $N \to \infty$.

Since it can be shown that the approximate solution $\vec{\tilde{A}}^N$ depends continuously on $\mathbf{q}$, solutions exist to the problem $\mathbf{(ASIDP)}^N$ for each N. Having established the results of **Lemma 6**, we can now use standard arguments [10, 11] to prove the following theorem.

Theorem 2: Suppose that the hypotheses **[H-0]** to **[H-4]** hold and let $\hat{\mathbf{q}}^N$ be a solution of the problem $\mathbf{(ASIDP)}^N$. Then the sequence $\left\{\hat{\mathbf{q}}^N\right\}$ admits a convergent subsequence $\hat{\mathbf{q}}^{N_k}$ with $\hat{\mathbf{q}}^{N_k} \to \mathbf{q}^*$ as $N_k \to \infty$. Moreover, $\mathbf{q}^*$ is a solution of the problem **(SIDP)**.

We now turn to a particular implementation of the method presented above. Let $\{B_i^M(x_1)\}_{i=1}^M$ be the series of B-spline functions ([12]). To characterize the crack depth, the shape function $r(x_1)$ is represented as

$$x_2 = r(x_1; \mathbf{q}) = \sum_{i=0}^{M+1} q_i^M B_i^M(x_1) \quad \text{for } |x_1| \leq c < d_i \tag{59}$$

with $q_0^M = q_{M+1}^M = h_0$. In order to ensure the compactness of the parameter set Q ([**H-0**]), we impose constraints,

$$Q = \left\{ \mathbf{q} \in R^M \mid \beta \leq q_i \leq h_0 \;\; i = 1, 2, \cdots, M \right\}. \tag{60}$$

Remark: The defect shape function satisfies the hypotheses **[H-1]** to **[H-4]**.

For the state approximation, let us choose $\cup_{N=1}^{\infty} \{\psi_i^N\}_{i=1}^N$ as a set of basis functions in $\tilde{V}$. (In the calculations reported on below, we used piecewise linear finite elements.) That is, for each N, $\{\psi_i^N\}_{i=1}^N$ are linearly independent and $\cup_N span\{\psi_i^N\}_{i=1}^N$ is dense in $L^2(G_0 \cup \tilde{G}_s^1 \cup \tilde{G}_s^2)$. Then the approximate subspaces can be chosen as $\hat{H}^N = H^N \times H^N$ where $H^N = span\{\hat{\psi}_i^N\}_{i=1}^{2N}$. Thus we can reconstruct the basis function by

$$\hat{\psi}_i^N = \begin{cases} (\psi_i^N, 0) & \text{for} \quad i = 1, 2, \cdots, N \\ (0, \psi_{i-N}) & \text{for} \quad i = N+1, N+2, \cdots, 2N \end{cases}.$$

An approximate solution can be then defined by

$$\vec{\tilde{A}}^N := \sum_{i=1}^{2N} w_i^N \hat{\psi}_i^N$$

where the coefficient vector $w^N = \{w_i^N\}_{i=1}^{2N}$ is chosen such that, for $j = 1, 2, \cdots 2N$,

$$\tilde{a}(\mathbf{q})(\sum_{i=1}^{2N} w_i^N \hat{\psi}_i^N, \hat{\psi}_j^N) = \tilde{L}(\mathbf{q})(\hat{\psi}_j^N).$$

Hence the system can be approximated by solving the linear system

$$K^N(\mathbf{q}) w^N = f^N(\mathbf{q}) \tag{61}$$

where

$$[K^N(\mathbf{q})]_{i,j} := \tilde{a}(\mathbf{q})(\hat{\psi}_i^N, \hat{\psi}_j^N) \quad \text{for} \quad i, j = 1, 2, \cdots, 2N$$

and where

$$[f^N(\mathbf{q})]_j := \tilde{L}(\mathbf{q})(\hat{\psi}_j^N) \quad \text{for} \quad j = 1, 2, \cdots, 2N.$$

The corresponding output can be computed as

$$\tilde{z}^N(\mathbf{q}; \omega_i) = \tilde{\mathcal{H}}^N w^N(\mathbf{q}; \omega_i) \quad (i = 1, 2, \cdots, M_o) \tag{62}$$

where

$$[\tilde{\mathcal{H}}^N]_{i,j} := [\tilde{\mathcal{H}}^N]_i \hat{\psi}_j^N \quad \text{for} \quad i = 1, 2, \cdots, m; j = 1, 2, \cdots, 2N.$$

Our computational algorithm is to seek the parameter $\hat{\mathbf{q}}^N \in Q$ which minimizes

$$F^N(\mathbf{q}) = \frac{1}{2} \sum_{i=1}^{M_o} \left| \tilde{\mathcal{H}}^N w^N(\mathbf{q}; \omega_i) - z_d(\omega_i) \right|^2. \tag{63}$$

6 Computational Experiments

In the numerical experiments, the window, the suspect region, and the size of conducting material sample in Fig. 9 were preassigned as

Window (domain) :	$d = 0.350[m]$	$h = 0.240[m]$
Suspect region :	$c = 0.025[m]$	
Conducting Material :	$d_c = 0.025[m]$	$h_0 = 0.020[m]$

Assuming that the sample material was a carbon fiber reinforced plastic (CFRP), the conductivity σ_c and the permeability μ_0 were taken as $\sigma_c = 1 \times 10^6$ [S/m] and $\mu_0 = 4\pi \times 10^{-7}$ [H/m], respectively. In the numerical experiments, we assume that a single frequency was used, i. e.,, $M_0 = 1$ in (57). The alternating current J_s and the applied frequency $f = \omega/2\pi$ were respectively given by $J_s = 40$ [mA] and $f = 100[Hz]$. The number of observation points was set as $m = 30$ and the set of scanning positions of SQUID coil probe given by (14) were chosen as

$$\bar{x}_i^1 = -r + o_i - \epsilon \quad \bar{x}_i^2 = -r + o_i + \epsilon \quad (i = 1, 2, \cdots, 30)$$

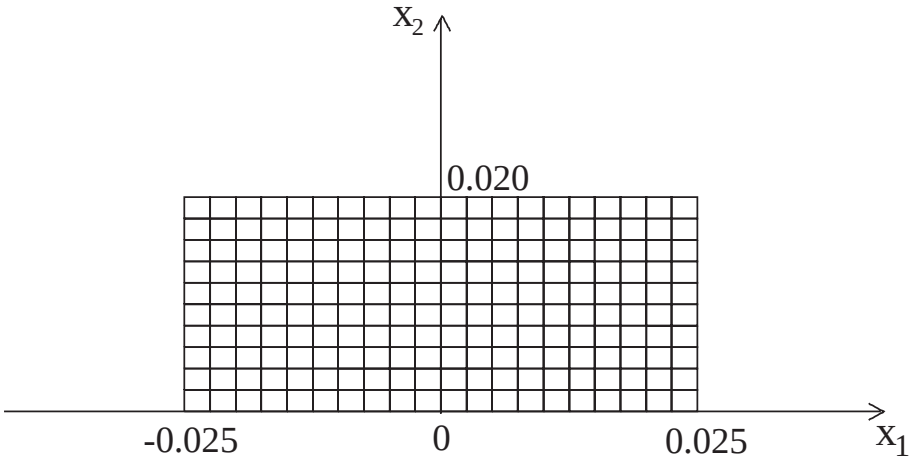

Figure 10: The decomposition of sample material

where

$$o_i = 0.0125 + 0.025i, \quad i = 1, 2, \cdots, 30,$$

and where ϵ denotes a sufficiently small positive value to restrict the effective area of the SQUID pick-up coil. The scanning line in Fig. 9 were set as $r = 0.0375[m]$ and $h_f = 0.003[m]$, respectively.

To discretize the system model by a finite-element method, the reference domain $G_0 \cup \tilde{G}_s^1 \cup \tilde{G}_s^2$ was divided into a finite number of elements $\{e_k\}_{k=1}^{K_e}$ and a number $N_e (> K_e)$ of nodes defined by $\{\tilde{\mathbf{x}}_i = (\tilde{x}_1^i,\ \tilde{x}_2^i)\}_{i=1}^{N_e}$ were selected in the reference domain. Each element is preassigned as an axiprallel rectangle with nodes at the vertices (see e. g., [13]). The number of finite elements and nodes in the numerical experiments reported in the sequel were set as $K_e = 3000 (= 50 \times 60)$ and $N_e = 3061 (= 51 \times 61)$ respectively. Figure 10 depicts the decomposition of the conducting material treated here. The number of elements and nodes in the material were taken as $200 (= 10 \times 20)$ and $231 (= 11 \times 21)$, respectively. Integration in the element matrices $K^N(\mathbf{q})$ and the element vector $f^N(\mathbf{q})$ were computed numerically by a Gauss-Legendre formula.

For these test example computations, simulated data $\{z_d\}$ were generated by first solving the finite-Galerkin model (61) and (62). A series of random Gaussian noise were added to the numerical solutions, thereby producing simulated noisy data for the algorithm. The essential difficulties in $(\mathbf{ASIDP})^N$ come from the fact that real data are heavily corrupted by observation noise and it often occurs that the corresponding model output data are far from those practical data. Tikhonov regularization is one possible technique for avoiding these serious difficulties in computational efforts. To this end, we adopt Tikhonov's regularization techniques to our inverse algorithm. More precisely, a regularization term is added to the cost functional (63) (see [14] for more details):

$$F_\eta^N(\mathbf{q}) = F^N(\mathbf{q}) + \frac{\eta}{2}\left|\mathbf{L_c q}\right|^2 \tag{64}$$

where

$$[\mathbf{L_c}]_{i,j} = \begin{bmatrix} 1 & -1 & 0 & \cdots & \cdots & 0 \\ 0 & 1 & -1 & 0 & \cdots & 0 \\ \vdots & 0 & \ddots & \ddots & & \vdots \\ \vdots & \vdots & & \ddots & \ddots & 0 \\ 0 & 0 & \cdots & 0 & 1 & -1 \end{bmatrix} \quad \in \; R^{(M-1)\times M}$$

In order to select the "optimal" parameter η, we used L-curve analysis (see [15, 16]). The outline of this approach in these experiments is summarized as follows:

[L-curve analysis] : Given $\eta \in [0, \infty)$, solve

$$F_\eta^N(\hat{\mathbf{q}}(\eta)) = \min_q F_\eta^N(\mathbf{q}), \tag{65}$$

for each fixed $\eta \in [0, \infty)$, collect the points

$$\left(\left|\tilde{z}^N(\hat{\mathbf{q}}_\eta; \omega) - z_d(\omega)\right|^2, \left|\mathbf{L_c}\hat{\mathbf{q}}_\eta\right|^2\right) \tag{66}$$

and plot the above points. Then the "optimal" parameter η^0 can be chosen as a point that lies in the "corner" of the resulting curve.

Evaluation of the vector gradient of the cost function (65) is the computationally expensive part of our algorithm. This can be accomplished by using a co-state approach. For the numerical results reported in this paper, we used the gradient projection method ([17]) which is a particularly useful technique for optimization problems with linear inequality constraints such as those in (60). The iterative algorithm for finding $\hat{\mathbf{q}}^N$ in this experiment is the same as that in [5].

In our test examples, we considered corrosion shape identification for conducting material samples with corrosion-like damage (of varying corrosion shape) as depicted in Fig. 6. The parameter function (59) to be identified is a piecewise linear spline function. We denote the knot sequence for r by

$$-0.025 = \tau_0^M < \tau_1^M < \cdots < \tau_{M+1}^M = 0.025$$

and the unknown parameter vector $\mathbf{q}^M = \{q_i^M\}_{i=1}^M$ is then given by

$$q_i^M = r(\tau_i^M) \quad \text{for } i = 1, 2, \cdots, M.$$

For the computational experiments, the dimensions of unknown parameter vector $\mathbf{q}$ was taken as $M = 19$. The lower bound in (60) was chosen as $\beta = 0.001$. The initial guesses for the parameters were given by

$$q_i^M = h_0(= 0.02) \quad (i = 1, 2, \cdots, M)$$

which imply that there exists no corrosion in the material. Carrying out a number of numerical experiments, we checked the robustness of the algorithm with respect to noise for various kinds of corrosion type damages. Here we summarize the numerical results for two typical examples.

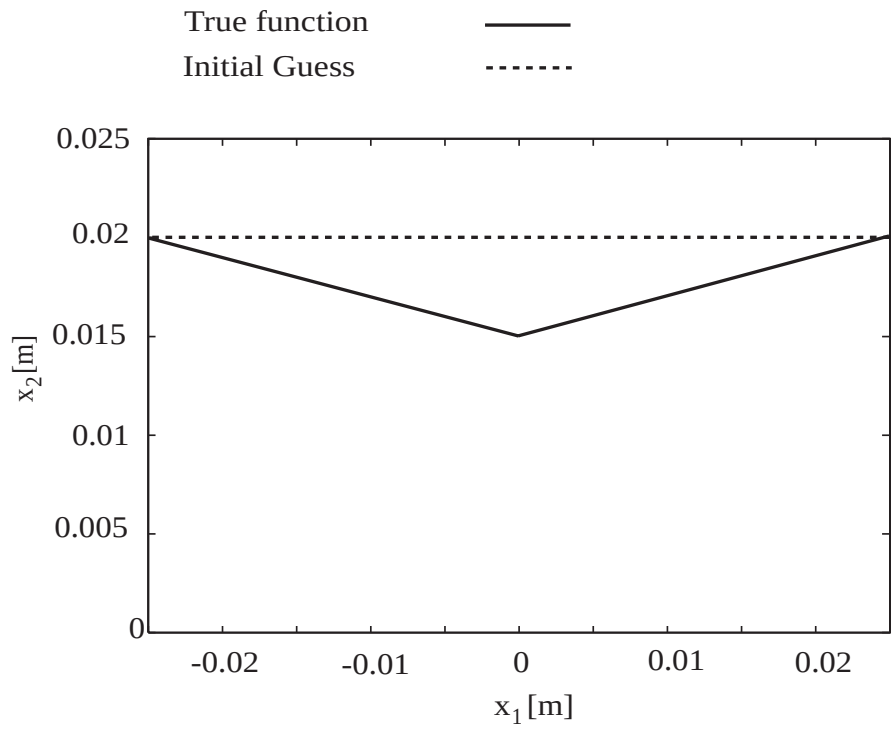

Figure 11: True function and estimated function in Example 1 (noise free)

Example 1: In this test example, we deal with the shape recovery for the CFRP sample with a symmetric type of corrosion as shown in Figure 11. The values of the true parameters were given by

$$q_1^{19} = q_{19}^{19} = 0.0195 \quad q_2^{19} = q_{18}^{19} = 0.0190 \quad q_3^{19} = q_{17}^{19} = 0.0185 \quad q_4^{19} = q_{16}^{19} = 0.0180$$
$$q_5^{19} = q_{15}^{19} = 0.0175 \quad q_6^{19} = q_{14}^{19} = 0.0170 \quad q_7^{19} = q_{13}^{19} = 0.0165 \quad q_8^{19} = q_{12}^{19} = 0.0160$$
$$q_9^{19} = q_{11}^{19} = 0.0155 \quad q_{10}^{19} = 0.0150.$$

The estimated parameters are listed in Table 1 using data that is with noise free, and with data containing 5%, 10%,and 20% relative noise. Fig. 12 depicts the L-curve for 5% noise case and $\eta^o = 5.0 \times 10^{-12}$ was chosen as the optimal regularization parameter in (64). The successful results is demonstrated in Fig. 13 that depicts the estimated shape using Tikhonov regularization with the optimal selection η^o and without the regularization.

Example 2: In this example, we deal with a somewhat more difficult case as compared to that of **Example-1**. The type of damage was given by a non-symmetric function as illustrated in Figure 14. We set the same dimension for the unknown parameter vector as in Example 1 and we also used the same knot sequence. The values of the true parameters were preassigned in

$$q_1^{19} = 0.0195 \quad q_2^{19} = 0.0190 \quad q_3^{19} = 0.0185 \quad q_4^{19} = 0.0180 \quad q_5^{19} = 0.0175$$
$$q_6^{19} = 0.0170 \quad q_7^{19} = 0.0165 \quad q_8^{19} = 0.0160 \quad q_9^{19} = 0.0155 \quad q_{10}^{19} = 0.0150$$

Table 1: True value and estimated values in Example 1

		$\tilde{q}_1$	$\tilde{q}_2$	$\tilde{q}_3$	$\tilde{q}_4$	$\tilde{q}_5$	$\tilde{q}_6$	$\tilde{q}_7$	$\tilde{q}_8$	$\tilde{q}_9$	$\tilde{q}_{10}$	$\tilde{q}_{11}$
True Value ($\times 10^{-2}$)		1.95	1.90	1.85	1.80	1.75	1.70	1.65	1.60	1.55	1.50	1.55
Initial Guess ($\times 10^{-2}$)		2.00	2.00	2.00	2.00	2.00	2.00	2.00	2.00	2.00	2.00	2.00
Noise	iteration 10	1.97	1.93	1.89	1.84	1.79	1.74	1.69	1.64	1.58	1.53	1.58
Free	iteration 20	1.96	1.92	1.87	1.82	1.77	1.72	1.66	1.61	1.56	1.48	1.56
($\times 10^{-2}$)	iteration 30	1.95	1.91	1.86	1.81	1.76	1.70	1.66	1.61	1.56	1.48	1.56
5%	iteration 10	2.00	1.99	1.96	1.90	1.83	1.76	1.69	1.61	1.57	1.59	1.62
Noise	iteration 14	2.00	1.99	1.96	1.90	1.83	1.75	1.67	1.59	1.50	1.48	1.58
($\times 10^{-2}$)												
10%	iteration 8	2.00	1.99	1.96	1.91	1.85	1.78	1.71	1.63	1.63	1.68	1.69
Noise	iteration 13	2.00	1.99	1.96	1.90	1.83	1.75	1.66	1.57	1.42	1.53	1.72
($\times 10^{-2}$)												
20%	iteration 10	2.00	2.00	1.99	1.95	1.90	1.84	1.78	1.72	1.74	1.80	1.82
Noise	iteration 13	2.00	2.00	1.99	1.95	1.89	1.82	1.75	1.67	1.57	1.70	1.86
($\times 10^{-2}$)												

		$\tilde{q}_{12}$	$\tilde{q}_{13}$	$\tilde{q}_{14}$	$\tilde{q}_{15}$	$\tilde{q}_{16}$	$\tilde{q}_{17}$	$\tilde{q}_{18}$	$\tilde{q}_{19}$	$\frac{1}{19}\sum_{i\leq 19}\lvert q_i-\hat{q}_i\rvert^2$
True Value($\times 10^{-2}$)		1.60	1.65	1.70	1.75	1.80	1.85	1.90	1.95	
Initial Guess($\times 10^{-2}$)		2.00	2.00	2.00	2.00	2.00	2.00	2.00	2.00	
Noise	iteration 10	1.64	1.69	1.74	1.79	1.84	1.89	1.93	1.97	1.26×10^{-5}
Free	iteration 20	1.61	1.66	1.72	1.77	1.82	1.87	1.92	1.96	2.62×10^{-6}
($\times 10^{-2}$)	iteration 30	1.61	1.66	1.71	1.76	1.81	1.86	1.91	1.95	9.19×10^{-7}
5%	iteration 10	1.64	1.69	1.77	1.84	1.89	1.94	1.97	2.00	5.11×10^{-5}
Noise	iteration 14	1.63	1.65	1.73	1.82	1.90	1.94	1.97	2.00	4.16×10^{-5}
($\times 10^{-2}$)										
10%	iteration 8	1.69	1.73	1.80	1.87	1.92	1.95	1.97	1.99	9.45×10^{-5}
Noise	iteration 13	1.64	1.62	1.73	1.85	1.92	1.96	1.97	1.99	7.19×10^{-5}
($\times 10^{-2}$)										
20%	iteration 10	1.81	1.82	1.86	1.91	1.95	1.98	1.99	1.99	2.62×10^{-4}
Noise	iteration 13	1.81	1.74	1.80	1.88	1.95	1.99	2.00	1.99	1.96×10^{-4}
($\times 10^{-2}$)										

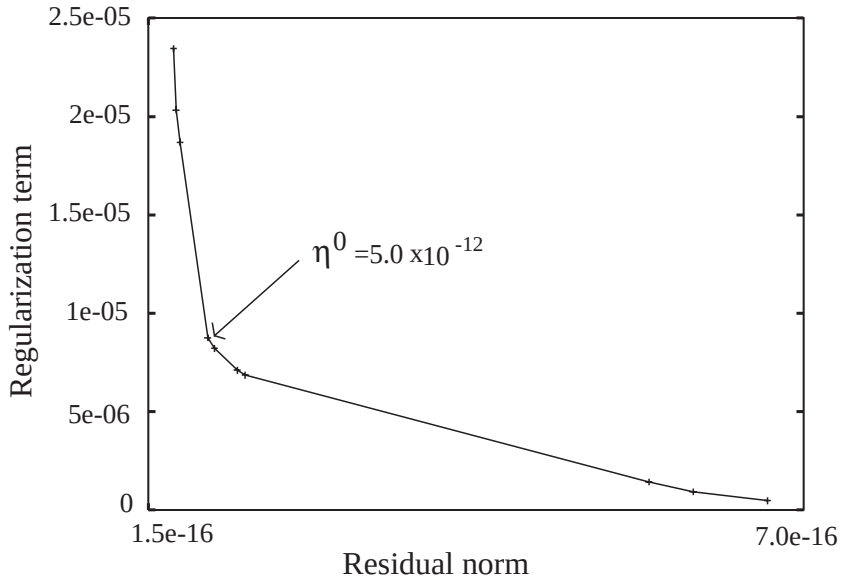

Figure 12: Tikhonov "L"-curve in Example 1 (5% noise)

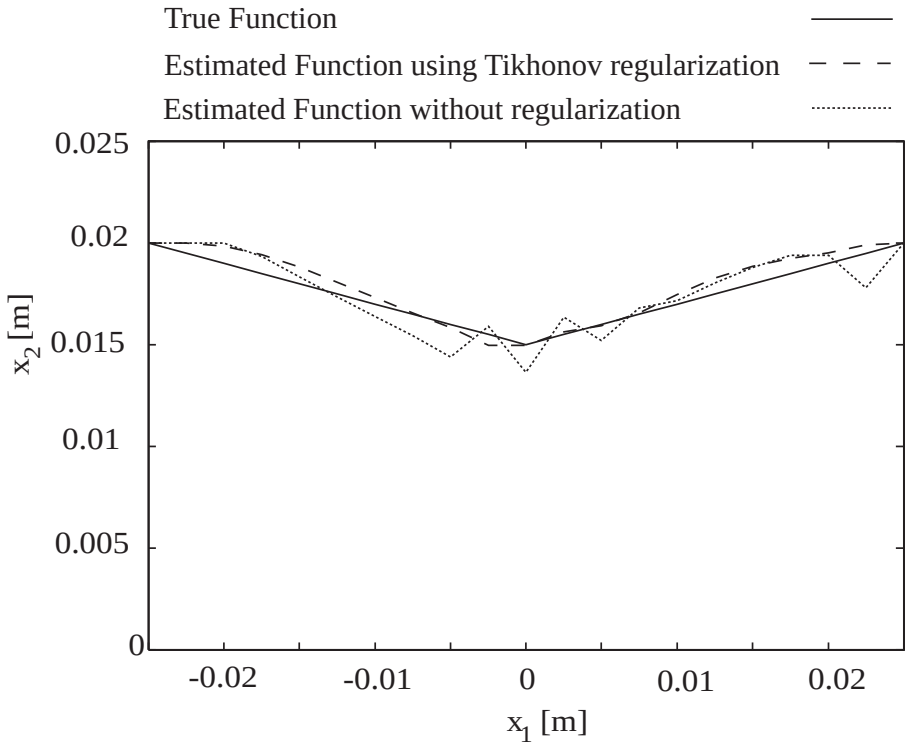

Figure 13: True function and estimated function in Example 1 (5% noise)

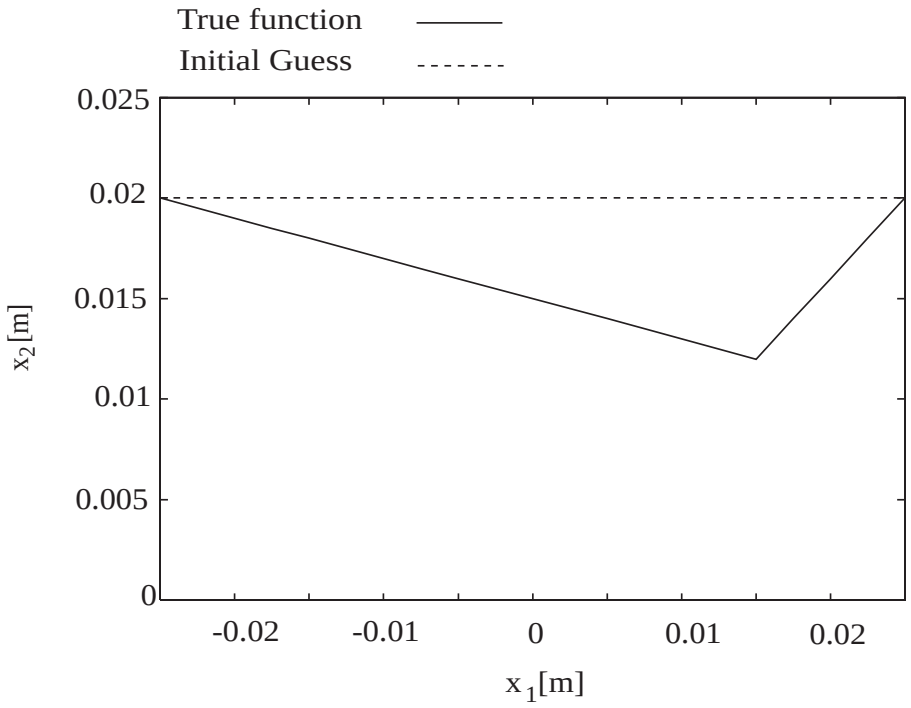

Figure 14: True function and estimated function in Example 2 (noise free)

$$q_{11}^{19} = 0.0145 \quad q_{12}^{19} = 0.0140 \quad q_{13}^{19} = 0.0135 \quad q_{14}^{19} = 0.0130 \quad q_{15}^{19} = 0.0125$$
$$q_{16}^{19} = 0.0120 \quad q_{17}^{19} = 0.0140 \quad q_{18}^{19} = 0.0160 \quad q_{7}^{19} = 0.0180.$$

The dimension of the unknown parameter vector and the number of observation points were chosen the same as in Example 1. Table 2 shows the estimated parameters for the data, that is, with noise free, and data with 5%, 10%, and 20% relative noise. Figure 15 depicts the Tikhonov L-curve for 5% noise case. Estimated corrosion shapes using Tikhonov regularization and without the regularization were demonstrated in Fig. 16.

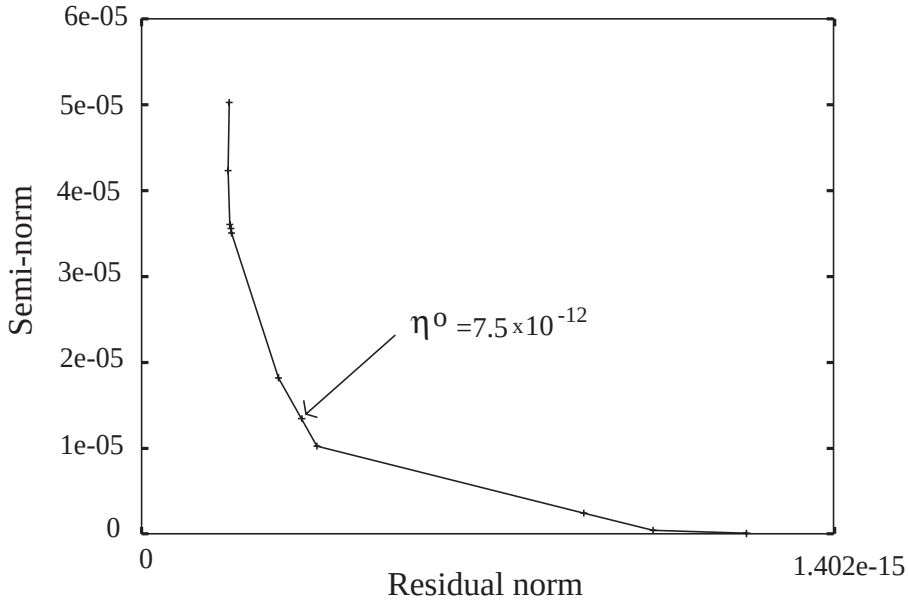

Figure 15: Tikhonov "L"-curve in Example 2 (5% noise)

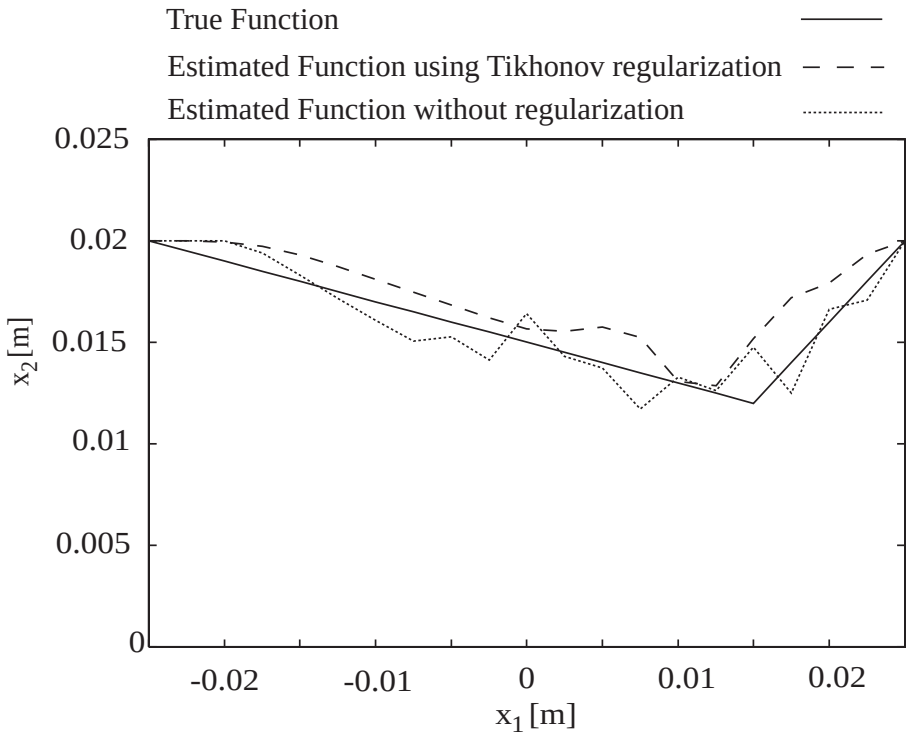

Figure 16: True function and estimated function in Example 2 (5% noise)

Table 2: True value and estimated values in Example 2

		$\tilde{q}_1$	$\tilde{q}_2$	$\tilde{q}_3$	$\tilde{q}_4$	$\tilde{q}_5$	$\tilde{q}_6$	$\tilde{q}_7$	$\tilde{q}_8$	$\tilde{q}_9$	$\tilde{q}_{10}$	$\tilde{q}_{11}$
True Value($\times 10^{-2}$)		1.95	1.90	1.85	1.80	1.75	1.70	1.65	1.60	1.55	1.50	1.45
Initial Guess($\times 10^{-2}$)		2.00	2.00	2.00	2.00	2.00	2.00	2.00	2.00	2.00	2.00	2.00
Noise Free ($\times 10^{-2}$)	iteration 10	1.99	1.97	1.94	1.90	1.86	1.81	1.77	1.72	1.67	1.62	1.57
	iteration 20	1.97	1.94	1.89	1.84	1.79	1.73	1.68	1.63	1.59	1.55	1.52
	iteration 190	1.92	1.93	1.85	1.80	1.74	1.72	1.63	1.58	1.54	1.49	1.45
5% Noise ($\times 10^{-2}$)	iteration 9	2.00	1.99	1.99	1.91	1.92	1.80	1.80	1.70	1.66	1.63	1.61
	iteration 12	2.00	2.00	1.97	1.93	1.87	1.81	1.75	1.68	1.62	1.57	1.55
10% Noise ($\times 10^{-2}$)	iteration 10	2.00	2.00	1.96	1.94	1.87	1.83	1.76	1.72	1.61	1.61	1.64
	iteration 13	2.00	2.00	1.97	1.93	1.87	1.81	1.75	1.68	1.60	1.50	1.59
20% Noise ($\times 10^{-2}$)	iteration 10	2.00	2.00	1.97	1.94	1.87	1.83	1.74	1.69	1.52	1.65	1.73
	iteration 13	2.00	2.00	1.98	1.93	1.87	1.80	1.73	1.63	1.48	1.49	1.78

		$\tilde{q}_{12}$	$\tilde{q}_{13}$	$\tilde{q}_{14}$	$\tilde{q}_{15}$	$\tilde{q}_{16}$	$\tilde{q}_{17}$	$\tilde{q}_{18}$	$\tilde{q}_{19}$	$\frac{1}{19}\sum_{i\leq 19}\lvert q_i - \hat{q}_i\rvert^2$
True Value($\times 10^{-2}$)		1.40	1.35	1.30	1.25	1.20	1.40	1.60	1.80	
Initial Guess($\times 10^{-2}$)		2.00	2.00	2.00	2.00	2.00	2.00	2.00	2.00	
Noise Free ($\times 10^{-2}$)	iteration 10	1.53	1.47	1.26	1.40	1.52	1.60	1.72	1.85	1.76×10^{-4}
	iteration 20	1.48	1.38	1.22	1.33	1.52	1.43	1.66	1.80	7.86×10^{-5}
	iteraton 190	1.42	1.36	1.29	1.19	1.38	1.35	1.55	1.75	2.43×10^{-5}
5% Noise ($\times 10^{-2}$)	iteration 9	1.59	1.52	1.37	1.47	1.62	1.70	1.78	1.92	3.13×10^{-4}
	iteration 12	1.58	1.52	1.31	1.29	1.52	1.72	1.79	1.93	2.24×10^{-4}
10% Noise ($\times 10^{-2}$)	iteration 10	1.63	1.51	1.41	1.55	1.70	1.77	1.80	1.92	4.08×10^{-4}
	iteration 13	1.66	1.54	1.31	1.40	1.65	1.80	1.81	1.91	3.45×10^{-4}
20% Noise ($\times 10^{-2}$)	iteration 10	1.66	1.53	1.55	1.68	1.79	1.85	1.85	1.91	6.17×10^{-4}
	iteration 13	1.73	1.49	1.40	1.58	1.78	1.88	1.85	1.90	5.71×10^{-4}

7 Concluding Remarks

A computational method was considered for the nonlinear output least square problem arising in electromagnetic nondestructive testing based on SQUID measurements. An important feature of the problem treated here was the use of a method of mapping technique for identifying the corrosion shape on the back surface of the conducting material. This method was effectively used both in the theoretical convergence for approximating identification problems and in the related computational methods. The practical utility of our computational algorithm is demonstrated through a series of numerical experiments as summarized in the previous section. Carrying out a large number of other numerical tests in addition to those reported for Examples 1 and 2, we report that the algorithm performed quite well for various noise levels. In the numerical experiments, robustness of the algorithm with respect to observation noise in the simulated data was demonstrated. A graphical method was also tested for determining the Tikhonov parameter by using the L-curve method. In all cases, our computational packages performed very well up to 5% noise level. We are currently pursuing computational experiments with laboratory data.

Acknowledgements.

This research was supported in part for the first author by the Air Force Office of Scientific Research under grant AFOSR F49620-01-1-0026. This research was also carried out in part while the second author was visiting at the Center for Research in Scientific Computations (CRSC), North Carolina State University. Additional support for the second author was also provided by the Japan Society for the Promotion Science under Grant No. 10680493.

References

[1] F. Kojima and N. Kasai: Data recovering technique for superconducting quantum interference device and its application to nondestructive evaluation; *Review of Progress in Quantitative Nondestructive Evaluation*, American Insitute of Physics Vol. 19B, pp. 1955-1962 (2000)

[2] H. T. Banks and F. Kojima: Boundary shape identification in two-dimensional electrostatic problems using SQUIDs; *Journal of Inverse and Ill-posed Problems*, Vol. 8, No. 5, pp. 487-504, (2000)

[3] Y. Hatsukade, N. Kasai, H. Takashima, R. Kawai, F. Kojima and A. Ishiyama: Development of NDE method using SQUID for reconstruction of defect shape; *IEEE Trans. Appl. Supercond.*, vol. 11, pp. 1311-1314 (2001)

[4] F. Kojima, R. Kawai, N. Kasai, and Y. Hatsukade: Defect profiles identification of conducting materials using HTS-SQUID gradiometer with multiple frequencies; *Review of Progress in Quantitative Nondestructive Evaluation*, vol. 20-A, pp. 377-384 (2001)

[5] H. T. Banks and F. Kojima: Boundary shape identification problems in two-dimensional domains related to thermal testing of materials; *Quarterly of Applied Mathematics*, Vol. XLVII, No. 2, pp. 273-293, (1989)

[6] H. T. Banks, F. Kojima, and W. P. Winfree: Boundary estimation problems arising in thermal tomography; *Inverse Problems*, Vol. 6, pp. 897-921, (1990)

[7] H. T. Banks, M. L. Joyner, B. Wincheski, and W.P. Winfree: Nondestructive evaluation using a reduced-order computational methodology; *Inverse Problems*, Vol. 16, pp. 929-945, (2000)

[8] M. L. Joyner: *An Application of a Reduced Order Computational Methodology for Eddy Current Based Nondestructive Evaluation Techniques*, Ph. D. Thesis, North Carolina State University, (2001)

[9] H. T. Banks, M. L. Joyner, B. Wincheski, and W.P. Winfree: Real time computational algorithms for eddy-current based damage detection; *Inverse Problems*, Vol. 18 (2002), to appear

[10] H.T. Banks, R.C. Smith and Y. Wang: *Smart Material Structures: Modeling, Estimation and Control*, John-Wiley/Masson, Chichester/Paris (1996).

[11] H. T. Banks, M. Buksas, anf T. Lin: *Electromagnetic Material Interrogation using Conductive Interfaces and Acoustic Wavefronts*, Frontiers in Applied Mathematics, Vol. FR21, SIAM, Philaderphia (2000)

[12] C. de Boor: *A Practical Guide to Splines*, Applied Mathematical Sciences, vol. 27, Springer-Verlag, New York (1978).

[13] O. Axelsson and V. A. Barker: *Finite Element Solution of Boundary Value Problems*, Academic Press, New York (1984) pp. 163-191.

[14] A. Tikhonov and V. Arseine: *Solutions of Ill-posed Problems*, John-Wiley, New York (1977).

[15] P.C. Hansen: Analysis of discrete ill-posed problems by means of L-curve; *SIAM Review*, Vol. 34, No. 4, pp. 561-580 (1992)

[16] F. Kojima: Robust analysis of boundary shape identification arising in thermal tomography; *Lecture Notes in RIMS, Kyoto University*, No. 836, pp. 78-87, (1993)

[17] J.B. Rosen: The gradient projection method for nonlinear programming, Part I: linear constraints; *SIAM J. Appl. Math.*, vol. 8, pp. 181-217 (1960).